

Design of origami structures with curved tiles between the creases

Huan Liu and Richard D. James

Department of Aerospace Engineering and Mechanics,
University of Minnesota, Minneapolis, MN 55455, USA
liu01003@umn.edu, james@umn.edu

Abstract. An efficient way to introduce elastic energy that can bias an origami structure toward desired shapes is to allow curved tiles between the creases. The bending of the tiles supplies the energy and the tiles themselves may have additional functionality. In this paper, we present the theorem and systematic design methods for quite general curved origami structures that can be folded from a flat sheet, and we present methods to accurately find the stored elastic energy. Here the tiles are allowed to undergo curved isometric mappings, and the associated creases necessarily undergo isometric mappings as curves. These assumptions are consistent with a variety of practical methods for crease design. The h^3 scaling of the energy of thin sheets ($h =$ thickness) spans a broad energy range. Different tiles in an origami design can have different values of h , and individual tiles can also have varying h . Following developments for piecewise rigid origami [1], we develop further the Lagrangian approach and the group orbit procedure in this context. We notice that some of the simplest designs that arise from the group orbit procedure for certain helical and conformal groups provide better matches to the buckling patterns observed in compressed cylinders and cones than known patterns.

Contents

1	Introduction	2
2	Necessary conditions that two isometrically deformed surfaces meet at a crease	4
2.1	Some results from differential geometry in Lagrangian form	4
2.2	Formulas for the rulings	6
2.3	Formulas for the creases	7
2.4	Formulas for isometrically deformed curved origami	8
3	Theorem on curved origami design	10
4	Curved origami design by the group orbit procedure	15
4.1	Helical groups	16
4.2	Circle groups	19
4.3	Translation groups	21
4.4	More on circle groups	23
4.5	Conformal groups	24

5	Curved tile generalizations of the Miura pattern	27
6	Energy of curved tiles	29
6.1	Kirchhoff’s nonlinear plate theory	29
6.2	Discussion of the folding motion and the energy landscape	30
7	Buckling patterns of thin-walled cylindrical and conical shells	33
A	Appendix	35
A.1	Proof of Theorem 5.1	35
A.2	Energy stored in a tangent surface	36

1 Introduction

An aspect of piecewise linear origami design appreciated by experts and recreational designers alike is the huge variety of ways a typical simple crease pattern can be folded. This friend of the recreational designer, and foe of the goal-oriented designer, is illustrated by the (fixed) crease pattern shown in Figure 3 of [2], having 16×16 tiles which can be folded 65,534 distinct ways, simply by varying the mountain-valley assignment on two adjacent edges of the unfolded pseudo-rectangular sheet.

This degeneracy can potentially be removed by adding appropriate elastic energy of the tiles by allowing them to bend. Great stiffness (or softness) can be achieved in this way [3, 4], but little is understood how this works. In addition, by engineering the thickness, tremendous freedom of the design of the energy landscape is possible for a single crease pattern, simply because of the h^3 ($h =$ thickness) dependence of energy on the thickness of the tiles, and the fact that different tiles can have different thicknesses. Even on a single tile, the thickness can be varied smoothly with position while preserving the property that the tile deforms isometrically, giving even more opportunity to design the energy landscape.

From a continuum mechanics viewpoint, the conventional approach to origami design can be described as Eulerian. One looks at the deformed configuration and identifies kinematic objects, like angles between neighboring tiles and distances, and then develops relationships between these qualities [5]. An elegant version of this approach making use of the isometric transformations and concepts from algebraic geometry is given in [6].

Our approach here is quite different and can be described as Lagrangian, though we frequently make use of concepts from the primarily Eulerian subject of differential geometry. The goal in this case is to give a formula for the deformation $\mathbf{y}(\mathbf{x})$, $\mathbf{x} \in \Omega$, or $\mathbf{y}(\mathbf{x}, t)$ in the dynamic case, where Ω is a flat reference configuration—typically a flat sheet with a crease pattern before folding. This approach has been developed in [7, 8, 9]; we develop further the Lagrangian method in the context of curved tile origami. We base the development on formulas for the rulings, and we find ways to include planar regions, inflection points, and straight segments on the crease that can occur for general isometric mappings (see [10, 11]). This gives quite a general Lagrangian framework to explore curved tile origami.

We also further develop a group orbit method for curved tile origami structures. The general idea was outlined in [12] as a method for constructing certain compatible microstructures arising from phase transformations in crystals and was developed for piecewise-linear origami structures in

[2, 8, 13]. This method relies on the isometry groups, which preserve curved isometric deformations. Different groups can be applied to the reference configuration and the deformed configuration, giving a variety of interesting structures. We further generalize this method by replacing isometry groups by conformal groups. These involve orthogonal transformations, translations, and dilatations. Fundamentally, the conformal group orbit method exploits the basic scaling law of nonlinear elasticity, $\mathbf{y}(\mathbf{x}, t) \rightarrow \eta \mathbf{y}((1/\eta)\mathbf{x}, (1/\eta)t)$, which preserves isometries, stress, equations of motion (with no body force), etc.

While exploring some of these examples, we noticed a striking resemblance between some of our structures to the buckling patterns observed in compressed cylindrical and conical shells (Section 7). In fact, the match is apparently much better than the Yoshimura and related patterns that are usually compared to these buckled states. While we do not pursue a detailed study of buckling and bifurcation here, these patterns do provide explicit “test functions” that would be essential for such a study, and we provide methods of calculation of their energies. It came as a surprise to us that other examples for conformal groups show a curious resemblance to various sea creatures studied originally by Thompson [14]. We do not know if this is purely coincidental, but we conjecture that the group structure plays a physiological role.

Curved tile origami structures are of longstanding interest from the many concepts proposed for deployable structures in space, that nevertheless have to be folded to fit into a space vehicle. But there is also rising interest from diverse areas: robotics [15, 16], foldable household and leisure items [17], medical devices [18], foldable buildings [19], wind turbines with deformable blades [20] and large scale structures that would be otherwise difficult to transport.

Table 1 Notation adopted in the paper

Notation	Description	Formula
Domain and Basis		
$\hat{\mathbf{y}}$	Isometric mapping	$\hat{\mathbf{y}} : \mathbb{R}^2 \rightarrow \mathbb{R}^3$
\mathbf{x}	Point in the reference flat domain	
\mathbf{y}	Point in the deformed domain	
$(\hat{\mathbf{e}}_1, \hat{\mathbf{e}}_2)$	Fixed orthonormal basis in \mathbb{R}^2	$\det(\hat{\mathbf{e}}_1, \hat{\mathbf{e}}_2) > 0$
(x_1, x_2)	Coordinates of \mathbf{x} in $(\hat{\mathbf{e}}_1, \hat{\mathbf{e}}_2)$	$\mathbf{x} = x_1 \hat{\mathbf{e}}_1 + x_2 \hat{\mathbf{e}}_2$
Variables in crease		
s	Arc length parameter of creases	$s \in \mathbb{R}, s_1 < s < s_2$
\mathbf{x}_0	Reference crease	$\mathbf{x}_0(s)$
\mathbf{x}'_0	Tangent vector of \mathbf{x}_0	$\mathbf{x}'_0(s)$
\mathbf{p}_0	Principal normal vector of \mathbf{x}_0 in \mathbb{R}^2	$\mathbf{x}'_0(s) \cdot \mathbf{p}_0(s) = 0,$ $\det(\mathbf{x}'_0(s), \mathbf{p}_0(s)) > 0$
κ_0	Curvature of \mathbf{x}_0	$\mathbf{x}''_0(s) \cdot \mathbf{p}_0(s)$
\mathbf{y}_0	Deformed crease	$\mathbf{y}_0(s)$
\mathbf{y}'_0	Tangent vector of \mathbf{y}_0	$\mathbf{y}'_0(s)$
\mathbf{p}	Principal normal vector of \mathbf{y}_0	
\mathbf{b}	Binormal vector of \mathbf{y}_0	$\mathbf{y}'_0(s) \times \mathbf{p}(s)$

κ	Curvature of \mathbf{y}_0	$\mathbf{y}_0''(s) \cdot \mathbf{p}(s)$
τ	Torsion of \mathbf{y}_0	$-\mathbf{b}'(s) \cdot \mathbf{p}(s)$
Variables in surface		
$\mathbf{y}_{,1}, \mathbf{y}_{,2}$	Derivatives of $\hat{\mathbf{y}}(\mathbf{x})$ w.r.t. x_1 and x_2	$\mathbf{y}_{,\sigma} = \frac{\partial \hat{\mathbf{y}}(\mathbf{x}(x_1, x_2))}{\partial x_\sigma}, \sigma = 1, 2$
\mathbf{e}	Reference rulings	
\mathbf{e}^\perp	Unit vector in \mathbb{R}^2 perpendicular to \mathbf{e}	$\mathbf{e} \cdot \mathbf{e}^\perp = 0,$ $\det(\mathbf{e}, \mathbf{e}^\perp) > 0$
\mathbf{t}	Deformed rulings	
\mathbf{t}^\perp	Unit vector perpendicular to \mathbf{t} lying in $\mathbf{t} - \mathbf{y}'_0$ plane	$\mathbf{t} \cdot \mathbf{t}^\perp = 0, \mathbf{t}^\perp \cdot \mathbf{y}'_0 > 0$
\mathbf{n}	Normal vector of a curved tile	$\mathbf{n} = \mathbf{y}_{,1} \times \mathbf{y}_{,2} = \mathbf{t} \times \mathbf{t}^\perp$
\mathbf{F}	Deformation gradient of $\hat{\mathbf{y}}$	$\nabla_{\mathbf{x}} \hat{\mathbf{y}}$
$\mathbf{e}_1, \mathbf{e}_2$	Reference rulings of the two tiles meeting at \mathbf{x}_0 in curved tile origami	
$\mathbf{e}_1^\perp, \mathbf{e}_2^\perp$	Unit vectors in \mathbb{R}^2 perpendicular to \mathbf{e}_σ	$\mathbf{e}_\sigma \cdot \mathbf{e}_\sigma^\perp = 0,$ $\det(\mathbf{e}_\sigma, \mathbf{e}_\sigma^\perp) > 0, \sigma = 1, 2$
$\mathbf{t}_1, \mathbf{t}_2$	Deformed rulings of the two tiles meeting at \mathbf{y}_0 in curved tile origami	
$\mathbf{t}_1^\perp, \mathbf{t}_2^\perp$	Unit vectors perpendicular to \mathbf{t}_σ lying in $\mathbf{t}_\sigma - \mathbf{y}'_0$ plane	$\mathbf{t}_\sigma \cdot \mathbf{t}_\sigma^\perp = 0,$ $ \mathbf{t}_\sigma^\perp \cdot \mathbf{y}'_0 > 0, \sigma = 1, 2$
$\mathbf{n}_1, \mathbf{n}_2$	Unit normal vectors of the two tiles in curved tile origami	
$\mathbf{F}_1, \mathbf{F}_2$	Deformation gradients of the two tiles in curved tile origami	
γ	The angle between \mathbf{n}_1 and \mathbf{p}	$\gamma \in (-\frac{\pi}{2} + \varepsilon, \frac{\pi}{2} - \varepsilon), \varepsilon > 0$
ρ_1, ρ_2	C^1 bounded functions	$\tau = \rho_1 \kappa, \gamma' = \rho_2 \kappa$
f_1, f_2	C^1 bounded functions	$\tau = f_1 \kappa \cos \gamma,$ $\gamma' = f_2 \kappa \cos \gamma$

2 Necessary conditions that two isometrically deformed surfaces meet at a crease

2.1 Some results from differential geometry in Lagrangian form

In this section, we collect some results from classical differential geometry for the convenience of the reader, and we rewrite some of these results in Lagrangian form. In fact, for our constructions in the sequel, our main tools are the two formulas for the rulings in the reference and deformed configurations and the invertible deformation that relates them. It will be seen that these formulas apply in large domains (with certain restrictions) and deliver exact isometric mappings. For Section 2.1 our presentation is informal; we work on a neighborhood of a point on a crease with smoothness

assumed as needed. Precise sufficient conditions that two smooth surfaces meet at a crease are given in Section 3.

Consider a smooth deformation $\mathbf{y} : \Omega \rightarrow \mathcal{S}$ from a domain $\Omega \subset \mathbb{R}^2$ into a generally curved surface $\mathcal{S} = \mathbf{y}(\Omega) \subset \mathbb{R}^3$. It will be convenient to use rectangular Cartesian components (x_1, x_2) relative to a fixed right-handed orthonormal basis $(\hat{\mathbf{e}}_1, \hat{\mathbf{e}}_2)$ for the domain Ω ,

$$\mathbf{x} = x_1 \hat{\mathbf{e}}_1 + x_2 \hat{\mathbf{e}}_2, \quad x_1, x_2 \in \mathbb{R}, \quad (1)$$

and a description in terms of vectors for the range.

We begin by deriving some local, necessary conditions for an isometric mapping. The deformation gradient $\mathbf{F} = \nabla_{\mathbf{x}} \mathbf{y}$ is given by

$$\mathbf{F} = \frac{\partial \mathbf{y}}{\partial x_i} \otimes \hat{\mathbf{e}}_i = \mathbf{y}_{,1} \otimes \hat{\mathbf{e}}_1 + \mathbf{y}_{,2} \otimes \hat{\mathbf{e}}_2, \quad (2)$$

where $\mathbf{y}_{,1}$ and $\mathbf{y}_{,2}$ are two tangent vectors of \mathcal{S} at $\mathbf{y}(\mathbf{x})$. From (2), they can be expressed as

$$\mathbf{y}_{,1} = \mathbf{F} \hat{\mathbf{e}}_1, \quad \mathbf{y}_{,2} = \mathbf{F} \hat{\mathbf{e}}_2. \quad (3)$$

By definition, if \mathbf{y} is an isometric mapping, it locally preserves lengths and angles in the sense that

$$\mathbf{F} \mathbf{x}_1 \cdot \mathbf{F} \mathbf{x}_2 = \mathbf{x}_1 \cdot \mathbf{x}_2 \quad (4)$$

for all $\mathbf{x}_1, \mathbf{x}_2 \in \Omega$. Substituting (3) into (4), we have the necessary and sufficient conditions

$$\mathbf{y}_{,1} \cdot \mathbf{y}_{,1} = \mathbf{y}_{,2} \cdot \mathbf{y}_{,2} = 1, \quad \mathbf{y}_{,1} \cdot \mathbf{y}_{,2} = 0, \quad (5)$$

for a mapping to be isometric. Clearly, a necessary and sufficient condition for (4) is

$$\mathbf{F}^T \mathbf{F} = \mathbf{I}. \quad (6)$$

Since $\mathbf{y}_{,i} \cdot \mathbf{y}_{,j} = \delta_{ij}$ by (5), we have the necessary condition for an isometric mapping,

$$\mathbf{y}_{,ik} \cdot \mathbf{y}_{,j} + \mathbf{y}_{,i} \cdot \mathbf{y}_{,jk} = 0. \quad (7)$$

Firstly, let $i = j$: we get $\mathbf{y}_{,ik} \cdot \mathbf{y}_{,i} = 0$ (no sum). Then let $j = k$: we get $\mathbf{y}_{,jj} \cdot \mathbf{y}_{,i} = 0$ (no sum). So we conclude from (7) that $\mathbf{y}_{,jk} \cdot \mathbf{y}_{,i} = 0$ for all $i, j, k = 1, 2$. For definiteness, we take the unit normal of \mathcal{S} to be $\mathbf{n} = \mathbf{y}_{,1} \times \mathbf{y}_{,2}$. Because $\mathbf{y}_{,i}$ are tangent vectors, we obtain

$$\mathbf{y}_{,jk} = y_{jk} \mathbf{n}, \quad j, k = 1, 2, \quad (8)$$

where $y_{ij} = \mathbf{y}_{,ij} \cdot \mathbf{n} = y_{ji}$ are the coefficients of the second fundamental form. Taking the gradient of \mathbf{F} , we have

$$\nabla \mathbf{F} = \mathbf{y}_{,ij} \otimes \hat{\mathbf{e}}_i \otimes \hat{\mathbf{e}}_j = \mathbf{n} \otimes (y_{ij} \hat{\mathbf{e}}_i \otimes \hat{\mathbf{e}}_j) \quad (9)$$

Since $\mathbf{y}_{,ij} \cdot \mathbf{y}_{,k} = 0$, we have $(\mathbf{y}_{,22} \cdot \mathbf{y}_{,1} - \mathbf{y}_{,12} \cdot \mathbf{y}_{,2})_{,1} + (\mathbf{y}_{,11} \cdot \mathbf{y}_{,2} - \mathbf{y}_{,12} \cdot \mathbf{y}_{,1})_{,2} = 0$. Expanding and simplifying above equation, we get

$$\mathbf{y}_{,11} \cdot \mathbf{y}_{,22} - \mathbf{y}_{,12} \cdot \mathbf{y}_{,21} = y_{11} y_{22} - y_{12}^2 = 0, \quad (10)$$

so at least one eigenvalue of the 2×2 matrix y_{ij} is 0. Hence, y_{ij} is a symmetric matrix of rank one and can be written as $y_{ij} = \Lambda m_i m_j$, where $m_1^2 + m_2^2 = 1$. The two eigenvalues 0 and Λ are the principal curvatures of the isometrically deformed surface. Defining the unit vector $\mathbf{e}^\perp = m_1 \hat{\mathbf{e}}_1 + m_2 \hat{\mathbf{e}}_2$, (9) becomes

$$\nabla \mathbf{F} = \Lambda \mathbf{n} \otimes \mathbf{e}^\perp \otimes \mathbf{e}^\perp. \quad (11)$$

Continuing with our local analysis, we assume by possibly shrinking Ω that $\Lambda \neq 0$ on Ω^\perp . Then, m_1, m_2 can be chosen to be continuously differentiable on Ω , and we obtain a continuously differentiable, right-handed, orthonormal basis field $(\mathbf{e}, \mathbf{e}^\perp)$ on Ω , where $\mathbf{e} = m_2 \hat{\mathbf{e}}_1 - m_1 \hat{\mathbf{e}}_2$.

We now prove that $\operatorname{div} \mathbf{e}^\perp = 0$. We begin by eliminating Λ from (8) in the form $\mathbf{y}_{ij} = \Lambda m_i m_j \mathbf{n}$. Then we note that $\operatorname{div} \mathbf{F} = \mathbf{y}_{,11} + \mathbf{y}_{,22} = \Lambda \mathbf{n}$ from $m_1^2 + m_2^2 = 1$. From (11), we have $\nabla \mathbf{F} \mathbf{e}^\perp = \operatorname{div} \mathbf{F} \otimes \mathbf{e}^\perp$. Taking divergence of the above equation and canceling terms, we get

$$\nabla \mathbf{F} \cdot \nabla \mathbf{e}^\perp = (\operatorname{div} \mathbf{e}^\perp) \operatorname{div} \mathbf{F}. \quad (12)$$

Differentiating $\mathbf{e}^\perp \cdot \mathbf{e}^\perp = 1$, we get $\mathbf{e}^\perp \cdot \nabla \mathbf{e}^\perp = 0$, so $\nabla \mathbf{F} \cdot \nabla \mathbf{e}^\perp = 0$. Since $\operatorname{div} \mathbf{F} = \Lambda \mathbf{n} \neq 0$, we conclude that $\operatorname{div} \mathbf{e}^\perp = 0$ on Ω . Thus, by direct calculation, we have

$$\nabla \mathbf{e} \mathbf{e} = -(\operatorname{div} \mathbf{e}^\perp) \mathbf{e}^\perp = 0. \quad (13)$$

2.2 Formulas for the rulings

We examine the integral curves of the vector field $\mathbf{e}(\mathbf{x})$. We choose $\mathbf{x}_0 \in \Omega$ and solve the ordinary differential equation

$$\mathbf{x}'(v) = \mathbf{e}(\mathbf{x}(v)), \quad \mathbf{x}(0) = \mathbf{x}_0. \quad (14)$$

Under our hypotheses, there is a unique local solution. Differentiating with respect to v , we have that $\mathbf{x}''(v) = \nabla \mathbf{e} \mathbf{e} = 0$ by (13), so the solution of (14) are straight lines, $\mathbf{x}(v) = v \mathbf{e}(\mathbf{x}_0) + \mathbf{x}_0$.

The formulas for the rulings in the reference domain come from the simple observation that we can allow \mathbf{x}_0 to lie on the smooth curve $\mathbf{x}_0(s)$ as long as it is transversal to the vector field $\mathbf{e}(\mathbf{x})$. Choose a smooth curve $\mathbf{x}_0(s)$, $s_1 < s < s_2$, in Ω that is transversal to the vector field $\mathbf{e}(\mathbf{x})$. Without loss of generality, we can also assume an arc-length parameterization of this curve, so we have, say,

$$\mathbf{x}'_0(s) \cdot \mathbf{e}^\perp(\mathbf{x}_0(s)) > 0, \quad |\mathbf{x}'_0(s)| = 1, \quad s_1 < s < s_2. \quad (15)$$

Then, for each $s \in (s_1, s_2)$, we can solve the ordinary differential equation (14) with initial condition $\mathbf{x}(s, 0) = \mathbf{x}_0(s)$ yielding the solution,

$$\mathbf{x}(s, v) = \mathbf{x}_0(s) + v \mathbf{e}(s), \quad (16)$$

where $\mathbf{e}(s) = \mathbf{e}(\mathbf{x}_0(s))$. The formula (16) describes the rulings in the reference domain. Under our hypotheses, the rulings do not intersect, by uniqueness of the initial-value problem (14). They may not cover all of Ω , but also may extend well beyond Ω in the directions $\mathbf{e}(s)$ if the deformation is defined on a larger domain. In any case to proceed with the necessary conditions, we assume that Ω is further reduced so that the rulings are defined on all of Ω .

¹Some of our constructions below have $\Lambda = 0$ in parts of the domain, but the fact that the associated mappings are exact isometric mappings will be proved from the sufficient conditions given in Theorem 3.1 below.

By (11), the deformation gradient is constant along a ruling in the reference domain, i.e.,

$$\frac{d}{dv}\mathbf{F}(\mathbf{x}(s, v)) = \nabla\mathbf{F}(\mathbf{x}(s, v))\frac{\partial\mathbf{x}(s, v)}{\partial v} = \nabla\mathbf{F}(\mathbf{x}(s, v))\mathbf{e}(s) = 0. \quad (17)$$

So, with s fixed, $\mathbf{F}(\mathbf{x}(s, v)) = \mathbf{F}(\mathbf{x}_0(s))$ is constant along the ruling $\mathbf{x}(s, v)$. We consider $\mathbf{y}(s, v) = \hat{\mathbf{y}}(\mathbf{x}(s, v))$ parameterized by the reference ruling variables v, s . Therefore, we have by the chain rule

$$\frac{\partial}{\partial v}\mathbf{y}(s, v) = \mathbf{F}(\mathbf{x}(s, v))\mathbf{e}(s) = \mathbf{F}(\mathbf{x}_0(s))\mathbf{e}(s) =: \mathbf{t}(s), \quad (18)$$

and $\mathbf{t}(s)$ is a unit vector by (5). Integrating this relation, we have

$$\mathbf{y}(s, v) = \mathbf{y}_0(s) + v\mathbf{t}(s). \quad (19)$$

Since $\mathbf{y}_0(s)$ is the isometric image of the arclength parameterized curve $\mathbf{x}_0(s)$, then it is also parameterized by arclength with $|\mathbf{y}'_0(s)| = 1$.

Additional necessary conditions on the rulings follow from the fact that $\mathbf{F}(s) := \mathbf{F}(\mathbf{x}_0(s))$ is constant on a ruling. Differentiating $\hat{\mathbf{y}}(\mathbf{x}(s, v)) = \mathbf{y}(s, v)$ with respect to s , we have the condition

$$v(\mathbf{F}(s)\mathbf{e}'(s) - \mathbf{t}'(s)) = \mathbf{y}'_0(s) - \mathbf{F}(s)\mathbf{x}'_0(s), \quad (20)$$

which, combined with (18), implies that

$$\mathbf{F}(s)\mathbf{e}(s) = \mathbf{t}(s), \quad \mathbf{F}(s)\mathbf{x}'_0(s) = \mathbf{y}'_0(s), \quad \mathbf{F}(s)\mathbf{e}'(s) = \mathbf{t}'(s) \quad (21)$$

on Ω . Define $\mathbf{t}^\perp(s)$ by $\mathbf{t}^\perp(s) = \mathbf{n}(s) \times \mathbf{t}(s)$. Then $\mathbf{x}'_0(s)$ and $\mathbf{y}'_0(s)$ can be expressed as

$$\begin{aligned} \mathbf{x}'_0(s) &= (\mathbf{x}'_0 \cdot \mathbf{e})\mathbf{e}(s) + (\mathbf{x}'_0 \cdot \mathbf{e}^\perp)\mathbf{e}^\perp(s), \\ \mathbf{y}'_0(s) &= (\mathbf{y}'_0 \cdot \mathbf{t})\mathbf{t}(s) + (\mathbf{y}'_0 \cdot \mathbf{t}^\perp)\mathbf{t}^\perp(s). \end{aligned} \quad (22)$$

We use the first and second of (21), (22) and the fact that $\mathbf{F}^T\mathbf{F} = \mathbf{I}$ to get

$$\mathbf{x}'_0 \cdot \mathbf{e} = \mathbf{y}'_0 \cdot \mathbf{t}, \quad \mathbf{x}'_0 \cdot \mathbf{e}^\perp = \mathbf{y}'_0 \cdot \mathbf{t}^\perp, \quad (23)$$

$$\mathbf{F}(s) = \mathbf{t}(s) \otimes \mathbf{e}(s) + \mathbf{t}^\perp(s) \otimes \mathbf{e}^\perp(s). \quad (24)$$

Finally, the third condition of (21) applied to (24) gives

$$\mathbf{t}'(s) = (\mathbf{e}^\perp(s) \cdot \mathbf{e}'(s))\mathbf{t}^\perp(s), \quad (25)$$

which implies

$$\mathbf{t}'(s) \cdot (\mathbf{t}(s) \times \mathbf{t}^\perp(s)) = 0. \quad (26)$$

2.3 Formulas for the creases

In our main Theorem 3.1 below we use the Frenet-Serret formulas to define the crease $\mathbf{y}_0(s)$, $s_1 < s < s_2$. The tangent $\mathbf{y}'_0(s)$, principal normal $\mathbf{p}(s)$ and binormal $\mathbf{b}(s)$ of a smooth arclength-parameterized curve $\mathbf{y}_0(s)$ with (signed) curvature $\kappa(s)$ and torsion $\tau(s)$ satisfy the linear system of ordinary differential equations

$$\begin{aligned} \mathbf{y}''_0(s) &= \kappa(s)\mathbf{p}(s), & \mathbf{y}'_0(s_1) &= \bar{\mathbf{y}}', \\ \mathbf{p}'(s) &= -\kappa(s)\mathbf{y}'_0(s) + \tau(s)\mathbf{b}(s), & \mathbf{p}(s_1) &= \bar{\mathbf{p}}, \\ \mathbf{b}'(s) &= -\tau(s)\mathbf{p}(s), & \mathbf{b}(s_1) &= \bar{\mathbf{b}}. \end{aligned} \quad (27)$$

(The precise smoothness and other conditions on $\kappa(s)$ and $\tau(s)$ are given in Theorem 3.1.) If the initial conditions $(\bar{\mathbf{y}}'_0, \bar{\mathbf{p}}, \bar{\mathbf{b}})$ are right-handed orthonormal, then the functions $\mathbf{y}'_0, \mathbf{p}, \mathbf{b}$ remain orthonormal for $s_1 < s < s_2$ due to the fact that their pairwise dot products satisfy a system of linear ordinary differential equations (ODEs) in standard form with initial conditions

$$(|\mathbf{y}'_0|^2, |\mathbf{p}|^2, |\mathbf{b}|^2, \mathbf{y}'_0 \cdot \mathbf{p}, \mathbf{y}'_0 \cdot \mathbf{b}, \mathbf{p} \cdot \mathbf{b})|_{s=s_1} = (1, 1, 1, 0, 0, 0). \quad (28)$$

By direct observation, these equations continue to have the solution $(1, 1, 1, 0, 0, 0)$ for $s > s_1$. The right-handedness follows from the right-handedness of the initial data and the continuity of this solution.

We emphasize that, unlike typical books on differential geometry, we do not assume that the curvature (or the torsion) is non-negative, but we allow it to have both signs in Section 3. Then the Frenet-Serret formulas make sense as ordinary differential equations and give curves that may have complex arrays of inflection points or straight regions. This is essential: many of our designs below have creases with inflection points. Similarly, the normal and binormal are also continuously differentiable. The curve with (signed) curvature $\kappa(s)$ and torsion $\tau(s)$ can be obtained by integrating the tangent,

$$\mathbf{y}_0(s) = \bar{\mathbf{y}}_0 + \int_{s_1}^s \mathbf{y}'_0(r) dr. \quad (29)$$

A smooth reference crease $\mathbf{x}_0(s), s_1 < s < s_2$ in \mathbb{R}^2 can be defined by using two-dimensional Frenet-Serret formulas. That is, the tangent $\mathbf{x}'_0(s)$ and the principal normal $\mathbf{p}_0(s)$ with (signed) curvature $\kappa_0(s)$ satisfy

$$\begin{aligned} \mathbf{x}''_0(s) &= \kappa_0(s)\mathbf{p}_0(s), & \mathbf{x}'_0(s_1) &= \bar{\mathbf{x}}'_0, \\ \mathbf{p}'_0(s) &= -\kappa_0(s)\mathbf{x}'_0(s), & \mathbf{p}_0(s_1) &= \bar{\mathbf{p}}_0, \end{aligned} \quad (30)$$

with $\bar{\mathbf{x}}'_0 \cdot \bar{\mathbf{p}}_0 = 0$. Then, $\mathbf{x}'_0(s), \mathbf{p}_0(s)$ remain orthonormal on (s_1, s_2) . $\mathbf{x}_0(s)$ can be obtained by

$$\mathbf{x}_0(s) = \bar{\mathbf{x}}_0 + \int_{s_1}^s \mathbf{x}'_0(r) dr. \quad (31)$$

In the following contents, we consider $\mathbf{y}_0(s)$ and $\mathbf{x}_0(s)$ are curves that can be defined by (27) and (30), respectively.

2.4 Formulas for isometrically deformed curved origami

In this section, we collect some necessary conditions for curved tile origami such that the whole structure is developable, i.e., isometric to a subset of a plane. First of all, consider a curve $\mathbf{y}_0(s), s_1 < s < s_2$ lying on a curved developable surface $\mathbf{y}(s, v), s_1 < s < s_2, v_1 < v < v_2$ with normal $\mathbf{n}(s)$. Let $\mathbf{x}_0(s)$ be the preimage of $\mathbf{y}_0(s)$. Since $\mathbf{y}'_0 = \mathbf{F}\mathbf{x}'_0$ and $\mathbf{y}''_0 = \mathbf{F}\mathbf{x}''_0 + \nabla\mathbf{F}\mathbf{x}'_0\mathbf{x}'_0$, by substituting (2) and (11) we get $\mathbf{y}'_0 \cdot \mathbf{y}_{,\sigma} = \mathbf{x}'_0 \cdot \hat{\mathbf{e}}_\sigma$ and $\mathbf{y}''_0 \cdot \mathbf{y}_{,\sigma} = \mathbf{x}''_0 \cdot \hat{\mathbf{e}}_\sigma, \sigma = 1, 2$. Then

$$\begin{aligned} \kappa\mathbf{n} \cdot \mathbf{b} &= (\mathbf{y}_{,1} \times \mathbf{y}_{,2}) \cdot (\mathbf{y}'_0 \times \mathbf{y}''_0) \\ &= (\mathbf{y}'_0 \cdot \mathbf{y}_{,1})(\mathbf{y}''_0 \cdot \mathbf{y}_{,2}) - (\mathbf{y}''_0 \cdot \mathbf{y}_{,1})(\mathbf{y}'_0 \cdot \mathbf{y}_{,2}) \\ &= (\mathbf{x}'_0 \cdot \hat{\mathbf{e}}_1)(\mathbf{x}''_0 \cdot \hat{\mathbf{e}}_2) - (\mathbf{x}''_0 \cdot \hat{\mathbf{e}}_1)(\mathbf{x}'_0 \cdot \hat{\mathbf{e}}_2) \\ &= \mathbf{x}''_0 \cdot \mathbf{p}_0 = \kappa_0. \end{aligned} \quad (32)$$

Since $\mathbf{n} \cdot \mathbf{y}'_0 = 0$, \mathbf{n} can be expressed as

$$\mathbf{n} = \pm \cos \gamma \mathbf{p} + \sin \gamma \mathbf{b}, \quad (33)$$

where $\gamma \in (-\pi/2, \pi/2)$ satisfies

$$\kappa_0 = \kappa \sin \gamma. \quad (34)$$

Now consider two generally curved surfaces with distinct normal vectors \mathbf{n}_1 and \mathbf{n}_2 join at a curve $\mathbf{y}_0 \in C^2$. Assume the whole structure is isometric to a plane without overlapping, and let \mathbf{x}_0 be the preimage of \mathbf{y}_0 . Then (32) shows that $\kappa \mathbf{n}_1 \cdot \mathbf{b} = \kappa \mathbf{n}_2 \cdot \mathbf{b} = \kappa_0$. Without loss and generality, \mathbf{n}_1 and \mathbf{n}_2 can be given by

$$\mathbf{n}_1 = \cos \gamma \mathbf{p} + \sin \gamma \mathbf{b}, \quad \mathbf{n}_2 = -\cos \gamma \mathbf{p} + \sin \gamma \mathbf{b}. \quad (35)$$

(At straight crease segments, \mathbf{p} and \mathbf{b} can be specified in such a way that (35) remains satisfied.) Thus,

$$\mathbf{n}_2 = (-\mathbf{I} + 2\mathbf{b} \otimes \mathbf{b})\mathbf{n}_1. \quad (36)$$

According to (34) and (35), if \mathbf{y}_0 is given (i.e., κ , \mathbf{p} and \mathbf{b} are given), for each \mathbf{x}_0 (i.e., κ_0), there are only two developable surfaces with normal vectors $\mathbf{n}_1, \mathbf{n}_2$ that can go through \mathbf{y}_0 . If we assign a different reference crease \mathbf{x}_0 , we can get different pairs of developable surfaces.

To avoid a trivial folding (cf., Figure 2(b) below), we assume \mathbf{n}_1 and \mathbf{n}_2 are distinct, i.e., $|\mathbf{n}_1 \cdot \mathbf{n}_2| \leq 1 - 2\varepsilon^2 < 1$ for some $\varepsilon > 0$. Since $\mathbf{n}_1 \cdot \mathbf{n}_2 = \mathbf{n}_1 \cdot (-\mathbf{I} + 2\mathbf{b} \otimes \mathbf{b})\mathbf{n}_1 = 2(\mathbf{b} \cdot \mathbf{n}_1)^2 - 1 \leq 1 - 2\varepsilon^2$ and $\mathbf{b} \cdot \mathbf{n}_1 = \mathbf{b} \cdot \mathbf{n}_2$, we have $|\mathbf{b} \cdot \mathbf{n}_\sigma|^2 \leq 1 - \varepsilon^2 < 1$, $\sigma = 1, 2$. Via (35) this is equivalent to

$$|\mathbf{p} \cdot \mathbf{n}_\sigma| \geq \varepsilon > 0, \quad \sigma = 1, 2. \quad (37)$$

Let \mathbf{t}_1 and \mathbf{t}_2 denote the rulings of the two surfaces. We assume transversality, i.e., that the ruling $\mathbf{t}_\sigma(s)$ and tangent to the crease $\mathbf{y}'_0(s)$ do not become parallel:

$$|\mathbf{t}_\sigma^\perp \cdot \mathbf{y}'_0| \geq c > 0, \quad \sigma = 1, 2, \quad (38)$$

for some $0 < c \ll 1$. This appears to be quite natural in the case of origami design. Since $\mathbf{t}_\sigma \cdot \mathbf{n}_\sigma = 0$, $\mathbf{t}_1, \mathbf{t}_2$ can be expressed as

$$\begin{aligned} \mathbf{t}_1 &= \cos \alpha_1 \mathbf{y}'_0 - \sin \alpha_1 \mathbf{n}_1 \times \mathbf{y}'_0, & \mathbf{t}_2 &= \cos \alpha_2 \mathbf{y}'_0 - \sin \alpha_2 \mathbf{n}_2 \times \mathbf{y}'_0, \\ \mathbf{t}_1^\perp &= \sin \alpha_1 \mathbf{y}'_0 + \cos \alpha_1 \mathbf{n}_1 \times \mathbf{y}'_0, & \mathbf{t}_2^\perp &= \sin \alpha_2 \mathbf{y}'_0 + \cos \alpha_2 \mathbf{n}_2 \times \mathbf{y}'_0, \end{aligned} \quad (39)$$

where $\alpha_1 \in (-\pi + \hat{c}, -\hat{c})$ and $\alpha_2 \in (\hat{c}, \pi - \hat{c})$, $\hat{c} = \arcsin c$. The angles α_σ represent the angles between the rulings \mathbf{t}_σ and \mathbf{y}'_0 . Then α_1, α_2 satisfy the necessary conditions $\mathbf{t}'_1 \cdot \mathbf{n}_1 = 0$ and $\mathbf{t}'_2 \cdot \mathbf{n}_2 = 0$ from (26), which imply

$$\kappa \cos \gamma \cot \alpha_1 = \tau + \gamma', \quad \kappa \cos \gamma \cot \alpha_2 = -\tau + \gamma'. \quad (40)$$

Necessary and sufficient conditions that there exist bounded C^1 functions $\cot \alpha_1$ and $\cot \alpha_2$ are that there exist bounded C^1 functions ρ_1, ρ_2 satisfying

$$\tau = \rho_1 \kappa, \quad \gamma' = \rho_2 \kappa. \quad (41)$$

Here, we have also used (37).

3 Theorem on curved origami design

In this section, we present the main theorem of the paper. We consider the classic problem of origami design of two smooth surfaces meeting at a deformed crease, and we wish to design the crease pattern in the reference domain, i.e., a single flat sheet. These two smooth surfaces must be obtainable from isometric deformations of this reference domain. One would then like to predict the reference crease that deforms isometrically to the given deformed crease and the reference rulings that deform to the given deformed rulings. The latter can guide the folding process.

Under mild conditions of smoothness, this is easily accomplished for just one surface, and there are many such surfaces. (This is obvious because one can take any isometric mapping of a flat sheet and simply draw a curve on the deformed surface. Taking the inverse image of this curve gives a reference crease.) However, the addition of a second surface meeting the same crease becomes quite restrictive: under mild restrictions, the first surface and the deformed crease determine the second surface.

Under mild restrictions, Theorem 3.1 below treats two isometrically deformed surfaces meeting at a deformed crease, both obtained by isometric deformations of a flat sheet and both sharing the same reference crease.

Theorem 3.1. *Let curvature and torsion, $\kappa, \tau \in C^1(s_1, s_2)$ of the deformed crease be given satisfying $\tau = \rho_1 \kappa$, where ρ_1 is a bounded C^1 function. Let the deformed crease $\mathbf{y}_0 \in C^2(s_1, s_2)$ together with its principal normal and binormal $\mathbf{p}, \mathbf{b} \in C^2(s_1, s_2)$ be the unique solutions of the Frenet-Serret equations*

$$\begin{aligned} \mathbf{y}_0'' &= \kappa \mathbf{p}, & \mathbf{y}_0'(s_1) &= \bar{\mathbf{y}}_0', \\ \mathbf{p}' &= -\kappa \mathbf{y}_0' + \tau \mathbf{b}, & \mathbf{p}(s_1) &= \bar{\mathbf{p}}, \\ \mathbf{b}' &= -\tau \mathbf{p}, & \mathbf{b}(s_1) &= \bar{\mathbf{b}}, \end{aligned} \quad (42)$$

with given right-handed orthonormal initial values $\bar{\mathbf{y}}_0', \bar{\mathbf{p}}, \bar{\mathbf{b}}$. (Alternatively, give the deformed crease \mathbf{y}_0 with the indicated smoothness having curvature and torsion satisfying $\tau = \rho_1 \kappa$ and calculate \mathbf{p}, \mathbf{b} consistent with the Frenet-Serret equations.) We restrict the domain of \mathbf{y}_0 , if necessary, so that it does not intersect itself on $[s_1, s_2]$.

To define Surface 1 and Surface 2, let $\gamma(s) \in [-\frac{\pi}{2} + \varepsilon, \frac{\pi}{2} - \varepsilon]$, $\varepsilon > 0$, be a $C^1(s_1, s_2)$ function satisfying $\gamma' = \rho_2 \kappa$, where ρ_2 is a bounded $C^1(s_1, s_2)$ function. Let

$$\begin{aligned} \mathbf{n}_1 &= \cos \gamma \mathbf{p} + \sin \gamma \mathbf{b}, & \mathbf{n}_2 &= -\cos \gamma \mathbf{p} + \sin \gamma \mathbf{b}, \\ \mathbf{t}_1 &= \cos \alpha_1 \mathbf{y}_0' - \sin \alpha_1 \mathbf{n}_1 \times \mathbf{y}_0', & \mathbf{t}_2 &= \cos \alpha_2 \mathbf{y}_0' - \sin \alpha_2 \mathbf{n}_2 \times \mathbf{y}_0', \\ \mathbf{t}_1^\perp &= \sin \alpha_1 \mathbf{y}_0' + \cos \alpha_1 \mathbf{n}_1 \times \mathbf{y}_0', & \mathbf{t}_2^\perp &= \sin \alpha_2 \mathbf{y}_0' + \cos \alpha_2 \mathbf{n}_2 \times \mathbf{y}_0', \end{aligned} \quad (43)$$

where $\alpha_1 \in (-\pi, 0), \alpha_2 \in (0, \pi)$ are defined by

$$\alpha_1 = \cot^{-1} \left(\frac{\rho_1 + \rho_2}{\cos \gamma} \right), \quad \alpha_2 = \cot^{-1} \left(\frac{\rho_2 - \rho_1}{\cos \gamma} \right). \quad (44)$$

Define the reference crease \mathbf{x}_0 by the following ODEs:

$$\begin{cases} \mathbf{x}_0'' &= \kappa_0 \mathbf{p}_0, & \mathbf{x}_0'(s_1) &= \bar{\mathbf{x}}_0', \\ \mathbf{p}_0' &= -\kappa_0 \mathbf{x}_0', & \mathbf{p}_0(s_1) &= \bar{\mathbf{p}}_0, \end{cases} \quad (45)$$

where

$$\kappa_0 = \kappa \mathbf{n}_\sigma \cdot \mathbf{b} = \kappa \sin \gamma, \quad \sigma = 1, 2. \quad (46)$$

The reference rulings of Surface 1 and Surface 2 are then defined by

$$\mathbf{e}_\sigma = \cos \alpha_\sigma \mathbf{x}'_0 - \sin \alpha_\sigma \mathbf{p}_0, \quad (47)$$

$$\mathbf{e}_\sigma^\perp = \sin \alpha_\sigma \mathbf{x}'_0 + \cos \alpha_\sigma \mathbf{p}_0, \quad \sigma = 1, 2. \quad (48)$$

The parameterizations of Surfaces 1 and 2 in terms of creases and rulings are

$$\mathbf{x}_\sigma(s, v) = \mathbf{x}_0(s) + v\mathbf{e}_\sigma(s), \quad (49)$$

$$\mathbf{y}_\sigma(s, v) = \mathbf{y}_0(s) + v\mathbf{t}_\sigma(s), \quad \sigma = 1, 2 \quad (50)$$

respectively, with $(s, v) \in \Omega_\sigma$, where $\Omega_1 = \{(s, v) : s_1 < s < s_2, -v_1^-(s) < v < v_1^+(s)\}$, $\Omega_2 = \{(s, v) : s_1 < s < s_2, -v_2^-(s) < v < v_2^+(s)\}$, and, by the restrictions on α_1 and α_2 , $v_1^-(s), \dots, v_2^+(s) > 0$ on (s_1, s_2) are assigned such that there are no intersections between rulings.

Let $\hat{\mathbf{y}}_\sigma(\mathbf{x})$, $\sigma = 1, 2$, be the induced mappings between rulings:

$$\hat{\mathbf{y}}_\sigma(\mathbf{x}_\sigma(s, v)) = \mathbf{y}_\sigma(s, v), \quad (s, v) \in \Omega_\sigma. \quad (51)$$

Then the two mappings $\hat{\mathbf{y}}_1$ and $\hat{\mathbf{y}}_2$ are each isometric.

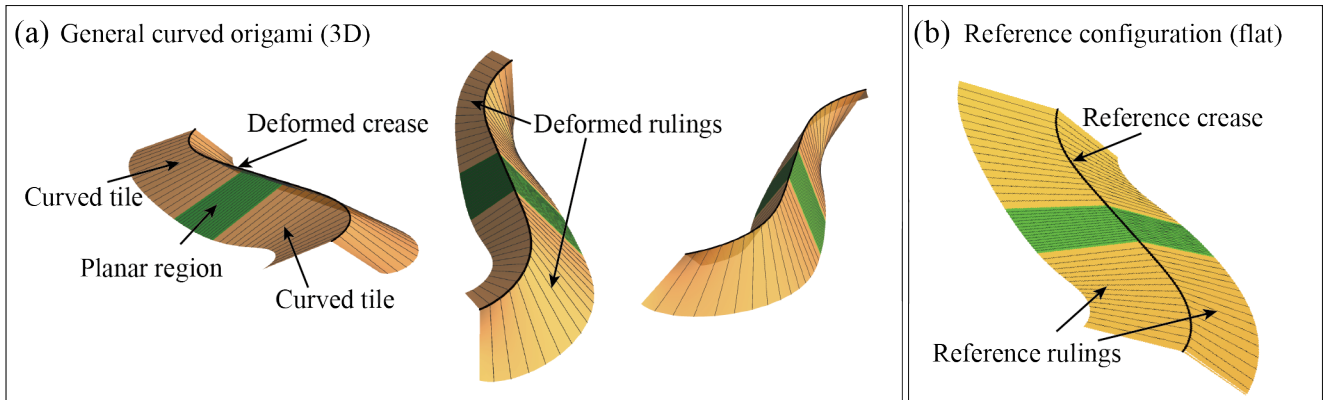


Figure 1: General curved origami given by Theorem 3.1 having planar regions (green). (a) Deformed configuration from three different viewpoints. (b) The reference configuration of (a). The surfaces highlighted in green in (a-b) are planar regions meeting at a straight crease segment. Note that the sheet in (b) is flat: the apparent bending at the crease is an optical illusion.

Proof. The formula (43) implies that $\{\mathbf{t}_\sigma, \mathbf{t}_\sigma^\perp, \mathbf{n}_\sigma\}$, $\sigma = 1, 2$ form two right-handed orthonormal bases. The formulas (44) are well defined since $\rho_1, \rho_2, \cos \gamma$ are bounded functions and the cotangent is invertible on $(-\pi, 0)$ and on $(0, \pi)$.

The invertibility of $\mathbf{x}_\sigma(s, v)$ on Ω_σ , $\sigma = 1, 2$ follows from the condition that the rulings do not intersect. By the smoothness and invertibility of $\mathbf{x}_\sigma(s, v)$, we have that $\hat{\mathbf{y}}_\sigma(\mathbf{x}_\sigma) \in C^1(\Omega_\sigma)$. Let the deformation gradient of $\hat{\mathbf{y}}_1$ be $\mathbf{F}_1 = \nabla_{\mathbf{x}_1} \hat{\mathbf{y}}_1$. Then \mathbf{F}_1 satisfies

$$\mathbf{y}'_0 + v\mathbf{t}'_1 = \mathbf{F}_1(\mathbf{x}'_0 + v\mathbf{e}'_1), \quad \mathbf{t}_1 = \mathbf{F}_1\mathbf{e}_1. \quad (52)$$

According to (43-44), $\mathbf{t}'_1, \mathbf{e}'_1$ are found by $\mathbf{t}'_1 = (\kappa_0 - \alpha'_1)\mathbf{t}_1^\perp$ and $\mathbf{e}'_1 = (\kappa_0 - \alpha'_1)\mathbf{e}_1^\perp$. Substituting to the first of (52), and since (52) is true for all $v \in (-v_1^-, v_1^+)$, one can get

$$\mathbf{y}'_0 - \mathbf{F}_1 \mathbf{x}'_0 = 0, \quad (\kappa_0 - \alpha'_1)(\mathbf{t}_1^\perp - \mathbf{F}_1 \mathbf{e}_1^\perp) = 0. \quad (53)$$

From (43) and (47-48), $\mathbf{y}'_0, \mathbf{x}'_0$ can be expressed as

$$\mathbf{y}'_0 = \cos \alpha_1 \mathbf{t}_1 + \sin \alpha_1 \mathbf{t}_1^\perp, \quad \mathbf{x}'_0 = \cos \alpha_1 \mathbf{e}_1 + \sin \alpha_1 \mathbf{e}_1^\perp. \quad (54)$$

Substitute (54) into the first of (53) and use the restriction on the domain of α_1 to get

$$\mathbf{t}_1^\perp = \mathbf{F}_1 \mathbf{e}_1^\perp, \quad (55)$$

which, together with the second of (52) ($\mathbf{t}_1 = \mathbf{F}_1 \mathbf{e}_1$), gives

$$\mathbf{F}_1 = \mathbf{t}_1 \otimes \mathbf{e}_1 + \mathbf{t}_1^\perp \otimes \mathbf{e}_1^\perp. \quad (56)$$

Since \mathbf{F}_1 satisfies $\mathbf{F}_1^T \mathbf{F}_1 = \mathbf{I}$ (cf., (6)), the mapping $\hat{\mathbf{y}}_1 : \mathbf{x}_1(\Omega_1) \rightarrow \mathbf{y}_1(\Omega_1)$ is isometric. Similarly, the deformation gradient for $\hat{\mathbf{y}}_2$ can be found by

$$\mathbf{F}_2 = \mathbf{t}_2 \otimes \mathbf{e}_2 + \mathbf{t}_2^\perp \otimes \mathbf{e}_2^\perp, \quad (57)$$

which implies the mapping $\hat{\mathbf{y}}_2 : \mathbf{x}_2(\Omega_2) \rightarrow \mathbf{y}_2(\Omega_2)$ is also isometric. \square

In brief, if \mathbf{y}_0 and the normal vector \mathbf{n}_1 of one surface are well defined under the assumptions in the theorem, this surface will be completely determined. The other surface is then determined by using its normal vector $\mathbf{n}_2 = (-\mathbf{I} + 2\mathbf{b} \otimes \mathbf{b})\mathbf{n}_1$ (see an example in Figure 2(a-b)). Specifying different \mathbf{n}_1 , one will get different pairs of surfaces, and the preimage \mathbf{x}_0 will change correspondingly. To get nontrivial curved origami structures, we assign the two mappings to each side of the crease, which gives two distinct deformed configurations, see Figure 2(c).

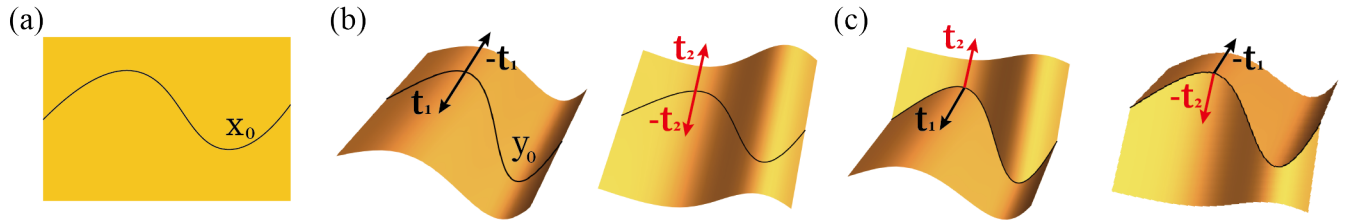


Figure 2: Examples of curved tile origami given by Theorem 3.1. (a) Reference domain. (b) Surface 1 and Surface 2 isometrically deformed from (a) going through \mathbf{y}_0 . The ruling directions on both sides of \mathbf{y}_0 are: $(\mathbf{t}_1, -\mathbf{t}_1)$ and $(-\mathbf{t}_2, \mathbf{t}_2)$. (c) Two curved origami structures by assigning these two mappings to different sides of the crease. The ruling directions on opposite sides of \mathbf{y}_0 are: $(\mathbf{t}_1, \mathbf{t}_2)$ and $(-\mathbf{t}_2, -\mathbf{t}_1)$.

In Theorem 3.1, one can assign κ, τ and the initial conditions in (42) to get a unique deformed crease \mathbf{y}_0 . Then different choices of γ will define different κ_0 (see 46), which give different reference creases \mathbf{x}_0 . Here we make two different choices of $\gamma(s)$, say $\gamma_1(s), \gamma_2(s)$, to get altogether four

surfaces passing through the crease \mathbf{y}_0 . Among these four, select one surface corresponding to γ_1 and another corresponding to γ_2 . In this way, we construct two different reference creases that deform to the same deformed crease and, correspondingly, two isometric mappings. This method applies to the case where the two reference regions are not compatible as shown in Figure 3(a). This case is exploited in famous architectural designs such as the Walt Disney Concert Hall in Los Angeles, California. Assume the two reference creases and the deformed crease are well prescribed. Then one can join two incompatible flat sheets with different creases together at the same deformed crease by solving each pair of reference crease and deformed crease individually. See Figure 3 for the four possibilities of this type.

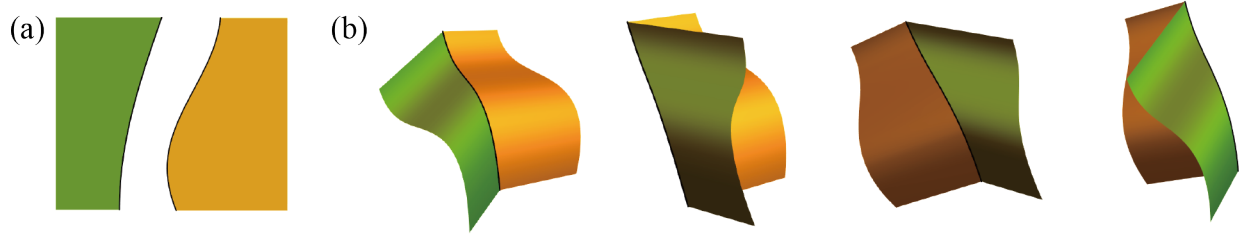


Figure 3: An example of generalized curved origami. (a) Incompatible reference domain. (b) The four branches of deformed configurations.

In summary, our methods contained in Theorem 3.1 treat quite generally cases analogous to classical origami, i.e., piecewise isometric folding a creased sheet (Figure 1 and Figure 2), or cases seen in Frank Gehry designed buildings (Figure 3) in which sheets bounded by two different reference creases are deformed isometrically to join at the same deformed crease.

The following series of corollaries follow immediately from Theorem 3.1.

Corollary 3.1. *Assume the hypotheses of Theorem 3.1. From (43), the normal vectors \mathbf{n}_1 and \mathbf{n}_2 satisfy*

$$\mathbf{n}_1 = -\mathbf{P}\mathbf{n}_2. \quad (58)$$

where $\mathbf{P} = \mathbf{I} - 2\mathbf{b} \otimes \mathbf{b}$. Substituting $\mathbf{t}_\sigma, \mathbf{t}_\sigma^\perp$ and $\mathbf{e}_\sigma, \mathbf{e}_\sigma^\perp$ into $\mathbf{F}_\sigma, \sigma = 1, 2$, \mathbf{F}_1 and \mathbf{F}_2 satisfy

$$\mathbf{F}_1 = \mathbf{P}\mathbf{F}_2, \quad (59)$$

i.e., the two deformation gradients \mathbf{F}_1 and \mathbf{F}_2 given by Theorem 3.1 are related by a reflection through a plane having normal given by the binormal of the crease.

Corollary 3.2. *Let \mathbf{y}_0 and γ be prescribed consistent with Theorem 3.1. Explicit formulas of quantities given by Theorem 3.1 for constructing curved origami are collected in Table 2. In the table, $f_1(s)$ and $f_2(s)$ are*

$$f_1 = \frac{\rho_1}{\cos \gamma}, \quad f_2 = \frac{\rho_2}{\cos \gamma}, \quad (60)$$

that is, f_1 and f_2 are bounded C^1 functions satisfying

$$\tau = f_1 \kappa \cos \gamma, \quad \gamma' = f_2 \kappa \cos \gamma. \quad (61)$$

Table 2: Formulas of constructing curved origami

Variable	Crease	
\mathbf{x}_0	$\int_{s_1}^s \left(\cos(\int_{s_1}^{\hat{s}} \kappa \sin \gamma dr) \hat{\mathbf{e}}_1 + \sin(\int_{s_1}^{\hat{s}} \kappa \sin \gamma dr) \hat{\mathbf{e}}_2 \right) d\hat{s}$	
\mathbf{x}'_0	$\cos(\int_{s_1}^s \kappa \sin \gamma dr) \hat{\mathbf{e}}_1 + \sin(\int_{s_1}^s \kappa \sin \gamma dr) \hat{\mathbf{e}}_2$	
\mathbf{p}_0	$-\sin(\int_{s_1}^s \kappa \sin \gamma dr) \hat{\mathbf{e}}_1 + \cos(\int_{s_1}^s \kappa \sin \gamma dr) \hat{\mathbf{e}}_2$	
	Surface 1	Surface 2
\mathbf{n}	$\cos \gamma \mathbf{p} + \sin \gamma \mathbf{b}$	$-\cos \gamma \mathbf{p} + \sin \gamma \mathbf{b}$
$\mathbf{n} \times \mathbf{y}'_0$	$\sin \gamma \mathbf{p} - \cos \gamma \mathbf{b}$	$\sin \gamma \mathbf{p} + \cos \gamma \mathbf{b}$
\mathbf{t}^\perp	$\frac{-\mathbf{y}'_0 - (f_1 + f_2)\mathbf{n}_1 \times \mathbf{y}'_0}{\sqrt{(f_1 + f_2)^2 + 1}}$	$\frac{\mathbf{y}'_0 - (f_1 - f_2)\mathbf{n}_2 \times \mathbf{y}'_0}{\sqrt{(f_1 - f_2)^2 + 1}}$
\mathbf{t}	$\frac{-(f_1 + f_2)\mathbf{y}'_0 + \mathbf{n}_1 \times \mathbf{y}'_0}{\sqrt{(f_1 + f_2)^2 + 1}}$	$\frac{-(f_1 - f_2)\mathbf{y}'_0 - \mathbf{n}_2 \times \mathbf{y}'_0}{\sqrt{(f_1 - f_2)^2 + 1}}$
\mathbf{e}^\perp	$\frac{-\mathbf{x}'_0 - (f_1 + f_2)\mathbf{p}_0}{\sqrt{(f_1 + f_2)^2 + 1}}$	$\frac{\mathbf{x}'_0 - (f_1 - f_2)\mathbf{p}_0}{\sqrt{(f_1 - f_2)^2 + 1}}$
\mathbf{e}	$\frac{-(f_1 + f_2)\mathbf{x}'_0 + \mathbf{p}_0}{\sqrt{(f_1 + f_2)^2 + 1}}$	$\frac{-(f_1 - f_2)\mathbf{x}'_0 - \mathbf{p}_0}{\sqrt{(f_1 - f_2)^2 + 1}}$

Corollary 3.3. *If \mathbf{y}_0 is a planar curve, then \mathbf{b} is constant and $\tau = 0$ on (s_1, s_2) . Thus, we can choose $f_1 = 0$ in Theorem 3.1. According to Table 2, the rulings satisfy*

$$\mathbf{t}_1 = -\mathbf{P}\mathbf{t}_2, \quad \mathbf{e}_1 = -\mathbf{e}_2. \quad (62)$$

Corollary 3.4. *In addition to constructing curved origami by specifying the deformed crease and one surface or by specifying the reference crease and the deformed crease, one can also specify the two distinct normal vectors $\mathbf{n}_1, \mathbf{n}_2$. Let $\mathbf{n}_1, \mathbf{n}_2 \in C^1$ be distinct normal vectors of the two surfaces satisfying $\mathbf{n}'_\sigma = \tau_\sigma \mathbf{t}_\sigma^\perp$, where $\tau_\sigma, \mathbf{t}_\sigma^\perp \in C^1, \sigma = 1, 2$. Since $\mathbf{y}'_0 \cdot \mathbf{n}_1 = 0$ and $\mathbf{y}'_0 \cdot \mathbf{n}_2 = 0$, the crease \mathbf{y}_0 is given by*

$$\mathbf{y}_0(s) = \bar{\mathbf{y}}_0 + \int_{s_1}^s \frac{\mathbf{n}_1 \times \mathbf{n}_2}{|\mathbf{n}_1 \times \mathbf{n}_2|} dr. \quad (63)$$

where $\hat{\mathbf{y}}_0 \in \mathbb{R}^3$. The transversality condition and the developability condition imply \mathbf{n}_1 and \mathbf{n}_2 satisfy

$$|(\mathbf{n}_1 \times \mathbf{n}_2) \cdot \mathbf{t}_\sigma^\perp| > 0, \quad (\mathbf{n}_{+1} \times \mathbf{n}_{-1}) \cdot (\mathbf{n}'_{+1} + \mathbf{n}'_{-1}) = 0. \quad (64)$$

By assigning the $\mathbf{n}_1, \mathbf{n}_2$ satisfying (64), one can construct curved origami structures using (63) and Table 2.

Corollary 3.5. *By direct calculation from (43), one can get that $\mathbf{t}_\sigma \parallel \mathbf{n}_\sigma \times \mathbf{n}'_\sigma, \sigma = 1, 2$. Assume $\mathbf{n}'_\sigma \neq 0$. Then \mathbf{t}_σ can be given by*

$$\mathbf{t}_\sigma = \mathbf{n}_\sigma \times \frac{\mathbf{n}'_\sigma}{|\mathbf{n}'_\sigma|}, \quad \sigma = 1, 2. \quad (65)$$

If \mathbf{n}_σ is a planar vector, \mathbf{t}_σ will be constant, which is the normal vector of the plane on which \mathbf{n}_σ is located.

Construction of more complicated structures then involves fitting these two-surface structures together, and the group orbit procedure described below is a suitable method for this purpose.

4 Curved origami design by the group orbit procedure

In this section we use a group orbit procedure to design complex origami structures, that is, origami structures are obtained by repeated application of a Euclidean group to an origami unit cell. A key idea is that elements of a Euclidean group preserve isometries. A second key idea is that Abelian Euclidean groups preserve the matching at creases. That is, matching of tiles at a few creases implies matching of tiles at all creases in the extended structure.

In this work, we will apply Abelian isometry groups that have been studied for piecewise linear origami in [2, 8, 13, 21]. The main difference between our present work and the earlier work is that in many cases our unit cells below contain interior creases, while in the earlier work the unit cells were typically single tiles. The presence of these additional creases gives us extra freedom that we exploit to describe a continuous folding path from a flat sheet to the folded structure.

A group element of a Euclidean group is written $g = (\mathbf{Q}|\mathbf{c})$, where $\mathbf{Q} \in \text{O}(3) = \{\mathbf{Q} : \mathbf{Q}^T \mathbf{Q} = \mathbf{I}\}$ and $\mathbf{c} \in \mathbb{R}^3$. The action of a group element on points $\mathbf{x} \in \mathbb{R}^3$ is given by $g(\mathbf{x}) = \mathbf{Q}\mathbf{x} + \mathbf{c}$. Below, we use the terminology ‘‘isometry’’ for the group elements $g = (\mathbf{Q}|\mathbf{c})$ or this action. The subgroup of $\text{O}(3)$ consisting of rotations is $\text{SO}(3) = \{\mathbf{R} \in \text{O}(3) : \det \mathbf{R} = 1\}$. We follow this notation below: \mathbf{Q} represents a typical element in $\text{O}(3)$ and \mathbf{R} represents an element in $\text{SO}(3)$. The multiplication rule for isometries is based on the composition of mappings using the action above, i.e., $g_1(g_2(\mathbf{x})) = g_1g_2(\mathbf{x})$ for all $\mathbf{x} \in \mathbb{R}^3$, and therefore is given by

$$g_1g_2 = (\mathbf{Q}_1|\mathbf{c}_1)(\mathbf{Q}_2|\mathbf{c}_2) = (\mathbf{Q}_1\mathbf{Q}_2|\mathbf{c}_1 + \mathbf{Q}_1\mathbf{c}_2). \quad (66)$$

The identity is $(\mathbf{I}|\mathbf{0})$.

While there are many Abelian isometry groups that we could use (see e.g., the International Tables of Crystallography [22]), we will focus on helical groups, circle groups and translation groups. We will later generalize these results to the conformal Euclidean groups, which involve also dilations and a suitable choice of product.

The main features of the unit cell for curved tile origami are: 1) as mentioned above, in most examples, we introduce an extra crease in the unit cell to gain some additional freedom; 2) we often use the rulings themselves as creases, e.g., $\overline{\mathbf{x}_a\mathbf{x}_b}$ and $\overline{\mathbf{x}_d\mathbf{x}_c}$ in Figure 4(a). The latter simplifies constructions: 3) since rulings are straight, we only have to be sure that two rulings related by

a group element are the same length; 4) regardless of the two isometric mappings meeting at a straight crease, the deformed structure will be compatible.

Following the choice of action above, we apply the group element $g = (\mathbf{Q}|\mathbf{c})$ to a suitable unit cell Ω in the following way: $g(\Omega) = \mathbf{Q}\Omega + \mathbf{c}$. After this group action, each unit cell with curved tiles should fit perfectly together with its neighbors. The beauty of Abelian groups is that, if this fitting is done only for the generators of the group, then the whole structure fits together perfectly. In short, the group builds the structure for you. Finally, for the groups involving global compatibility, such as the helical and circle groups, these groups should be discrete ([2, 8] and below), which will generate discrete and globally compatible curved origami.

Extending the notation used above, we use Ω and \mathcal{S} , respectively, to denote the unit cell before and after folding. The origami unit cell we choose will typically contain one inner curved crease $\mathbf{x}_1(s) \subset \Omega$ and two boundary creases $\mathbf{x}_0(s), \mathbf{x}_2(s) \subset \Omega$, all parameterized by $s \in (s_1, s_2)$, as shown in Figures 4-8(a). The isometric images of the three curves are $\mathbf{y}_1(s), \mathbf{y}_0(s)$ and $\mathbf{y}_2(s)$, respectively. Any two points on adjacent creases with the same s are connected by a ruling. A ruling between $\mathbf{y}_0(s)$ and $\mathbf{y}_1(s)$ has tangent $\mathbf{t}_1(s)$, and the ruling between $\mathbf{y}_1(s)$ and $\mathbf{y}_2(s)$ has tangent $\mathbf{t}_2(s)$. The deformation gradients of $\mathbf{t}_1(s)$ and $\mathbf{t}_2(s)$ are $\mathbf{F}_1(s)$ and $\mathbf{F}_2(s)$ respectively. The binormal vectors of the creases at $\mathbf{y}_i(s)$ are denoted by $\mathbf{b}_i(s), i = 0, 1, 2$. $\mathbf{P}_i(s) = \mathbf{I} - 2\mathbf{b}_i(s) \otimes \mathbf{b}_i(s)$ is a reflection tensor relating to the i^{th} crease. We use $\mathbf{x}_i, i = a, b, c, d$ to denote the four corner points of the reference unit cell and denote their images by $\mathbf{y}_i, i = a, b, c, d$, see Figures 4-8(a) and (c).

The general result we use repeatedly below is the following, described in the context of discrete Abelian isometry groups with two generators as in Figure 4. Let \mathcal{T} be the group applied to Ω with generators t_1 and t_2 , and let \mathcal{G} be the group applied to \mathcal{S} with generators of g_1 and g_2 . Let $\mathbf{x}_3(s) = \overline{\mathbf{x}_c\mathbf{x}_d}$, $\mathbf{x}_4(s) = \overline{\mathbf{x}_b\mathbf{x}_a}$ denote the remaining two sides of $\partial\Omega$ apart from $\mathbf{x}_0(s)$ and $\mathbf{x}_2(s)$. Suppose there is an isometric mapping $\mathbf{y} : \Omega \rightarrow \mathcal{S}$ satisfying $\mathbf{y}(\partial\Omega) = \partial\mathcal{S}$, that is, $\mathbf{y}(\mathbf{x}_i(s)) = \mathbf{y}_i(s), i = 0, 2, 3, 4$ (Figure 4(c)). Assume that, by adjusting the group parameters, we also arrange that

$$t_1(\mathbf{x}_0(s)) = \mathbf{x}_2(s), \quad t_2(\mathbf{x}_3(s)) = \mathbf{x}_4(s), \quad (67)$$

$$g_1(\mathbf{y}_0(s)) = \mathbf{y}_2(s), \quad g_2(\mathbf{y}_3(s)) = \mathbf{y}_4(s). \quad (68)$$

Now we apply the group \mathcal{T} , not just to $\partial\Omega$, but to all of Ω . By construction, by simply matching on two boundaries, we achieve that $\mathcal{T}(\Omega)$ is a perfect lattice of translated copies of Ω without gaps (Figure 4(b)). Similarly, $\mathcal{G}(\mathcal{S})$ is a perfect helical structure isometrically mapped from $\mathcal{T}(\Omega)$ (Figure 4(d)). If the group \mathcal{G} is discrete, the structure closes perfectly. That is, referring to Figure 4(d), discreteness for a helical group has the geometric interpretation that the helical structure can be produced by a ‘‘rolling up’’ construction, and, once rolled up, there is no seam. Equivalently, from a group theory perspective, discreteness means that the group acting on any point in \mathbb{R}^3 produces a family of points without accumulation points.

4.1 Helical groups

Helical origami is obtained by applying a helical group to a partially folded unit cell \mathcal{S} as shown in Figure 4. We consider helical groups with two generators

$$\mathcal{G}(\mathcal{S}) = \{g_1^p g_2^q(\mathcal{S}) : (p, q) \in \mathbb{Z}^2\}, \quad (69)$$

where g_1, g_2 are two screw isometries

$$g_1 = (\mathbf{R}_1|\tau_1\mathbf{e}_R + (\mathbf{I} - \mathbf{R}_1)\mathbf{z}), \quad g_2 = (\mathbf{R}_2|\tau_2\mathbf{e}_R + (\mathbf{I} - \mathbf{R}_2)\mathbf{z}), \quad (70)$$

with $\mathbf{R}_1, \mathbf{R}_2 \in \text{SO}(3)$, $\mathbf{R}_1 \neq \mathbf{I}$, $\mathbf{e}_R, \mathbf{z} \in \mathbb{R}^3$, $|\mathbf{e}_R| = 1$, $\tau_1, \tau_2 \in \mathbb{R}$, $\mathbf{z} \cdot \mathbf{e}_R = 0$ and $\mathbf{R}_1 \mathbf{e}_R = \mathbf{R}_2 \mathbf{e}_R = \mathbf{e}_R$. Let θ_1 and θ_2 denote the rotation angles of \mathbf{R}_1 and \mathbf{R}_2 , respectively. These parameters are subject to discreteness conditions

$$p^* \tau_1 + q^* \tau_2 = 0, \quad p^* \theta_1 + q^* \theta_2 = 2\pi, \quad (71)$$

where $(p^*, q^*) \in \mathbb{Z}^2$ is some pair of integers [21].

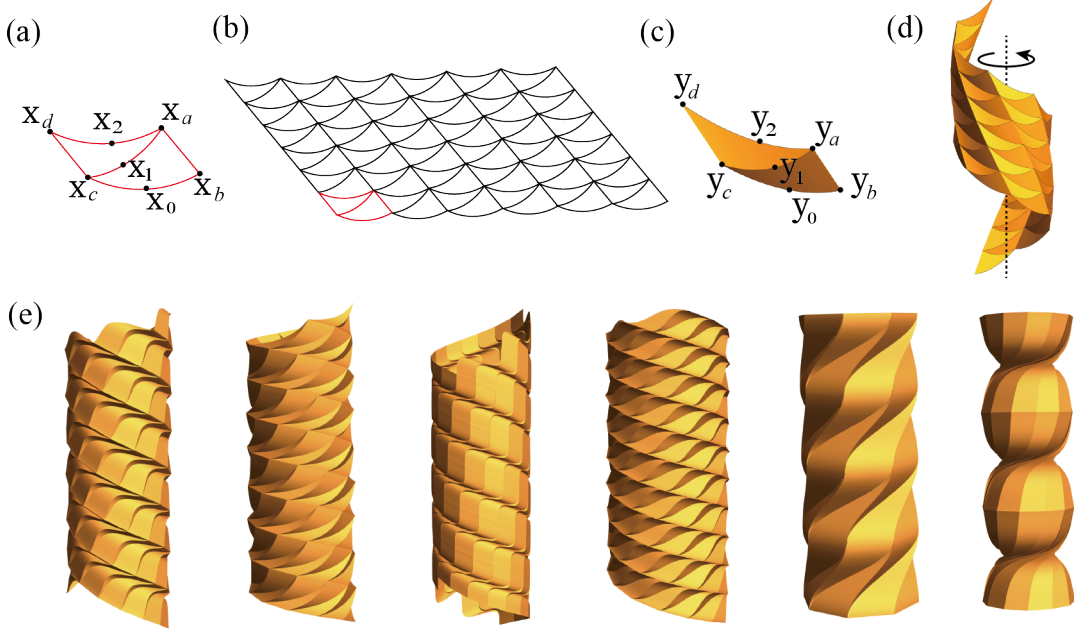


Figure 4: Curved tile origami generated by helical groups. (a) Reference unit cell. (b) Reference configuration. Note that (b) is flat sheet: the apparent curvature is an optical illusion. (c) Deformed unit cell. (d) Deformed configuration. (e) Some examples.

In the reference domain, the reference unit cell Ω shown in Figure 4(a) consists of two triangle-like flat regions that meet at the curved crease $\mathbf{x}_1(s)$, $s_1 < s < s_2$. The two boundary creases $\mathbf{x}_0(s)$ and $\mathbf{x}_2(s)$ differ by a translation. All creases satisfy the smoothness conditions of Theorem 3.1. The other two straight boundaries on the left- and right-handed sides are chosen to be two rulings after deformation. The overall reference domain can be obtained by a translation group

$$\mathcal{T}(\Omega) = \{t_1^p t_2^q(\Omega) : (p, q) \in \mathbb{Z}^2\}, \quad (72)$$

where

$$t_1 = (\mathbf{I}|\mathbf{c}_1), \quad t_2 = (\mathbf{I}|\mathbf{c}_2), \quad (73)$$

with $\mathbf{c}_1, \mathbf{c}_2 \in \mathbb{R}^3$ and $t_1^p t_2^q(\Omega) = \Omega + p\mathbf{c}_1 + q\mathbf{c}_2$, $p, q \in \mathbb{Z}$. See Figure 4(b), which is a curved-crease generalization of the Kresling pattern.

For a suitable unit cell, we apply \mathcal{T} to its reference configuration Ω and apply \mathcal{G} to its deformed configuration \mathcal{S} . The curved creases between adjacent unit cells should be compatible before and

after folding. Then, at the curved crease, we have the local compatibility conditions

$$\mathbf{x}_2(s) = t_1(\mathbf{x}_0(s)) = \mathbf{x}_0(s) + \mathbf{c}_1, \quad (74)$$

$$\mathbf{y}_2(s) = g_1(\mathbf{y}_0(s)) = \mathbf{R}_1\mathbf{y}_0(s) + \tau_1\mathbf{e}_R + (\mathbf{I} - \mathbf{R}_1)\mathbf{z}. \quad (75)$$

Thus, $\mathbf{x}'_2 = \mathbf{x}'_0$, $\mathbf{y}'_2 = \mathbf{R}_1\mathbf{y}'_0$. Combining with $\mathbf{y}'_0 = \mathbf{F}_1\mathbf{x}'_0$ and $\mathbf{y}'_2 = \mathbf{F}_2\mathbf{x}'_2$, we have $\mathbf{y}'_2 = \mathbf{R}_1\mathbf{F}_1\mathbf{x}'_2$, where \mathbf{F}_2 and $\mathbf{R}_1\mathbf{F}_1$ correspond to the deformation gradients of the surfaces on opposite sides of \mathbf{y}_2 . From Corollary 3.1, the deformation gradients satisfy $\mathbf{F}_2 = \mathbf{P}_1\mathbf{F}_1$ and $\mathbf{F}_2 = \mathbf{P}_2\mathbf{R}_1\mathbf{F}_1$. So

$$\mathbf{P}_2\mathbf{P}_1 = \mathbf{R}_1. \quad (76)$$

Since \mathbf{R}_1 is constant, we also have $\mathbf{y}''_2 = \mathbf{R}_1\mathbf{y}''_0$ from (75). Replacing \mathbf{R}_1 by $\mathbf{P}_2\mathbf{P}_1$ we have

$$\mathbf{y}'_2 = \mathbf{P}_2\mathbf{P}_1\mathbf{y}'_0 = \mathbf{P}_1\mathbf{y}'_0, \quad \mathbf{y}''_2 = \mathbf{P}_2\mathbf{P}_1\mathbf{y}''_0 = \mathbf{P}_1\mathbf{y}''_0. \quad (77)$$

Because $\mathbf{y}''_2 = (\mathbf{P}_1\mathbf{y}'_0)' = \mathbf{P}_1\mathbf{y}''_0 + \mathbf{P}'_1\mathbf{y}'_0$, we get $\mathbf{P}'_1\mathbf{y}'_0 = 0$, that is, $(\mathbf{b}_1 \cdot \mathbf{y}'_0)\mathbf{b}'_1 + (\mathbf{b}'_1 \cdot \mathbf{y}'_0)\mathbf{b}_1 = 0$. By simple argument, one can see \mathbf{b}_1 is constant. In the same way, we can conclude that $\mathbf{b}_0, \mathbf{b}_2$ are constant, which implies the creases $\mathbf{y}_0(s), \mathbf{y}_1(s)$, and $\mathbf{y}_2(s)$ are planar curves. According to Corollary 3.3 for planar creases, we get $\mathbf{t}_1 = -\mathbf{P}_1\mathbf{t}_2$ and $\mathbf{e}_1 = -\mathbf{e}_2$. Since the rulings in the whole reference domain are periodic, the reference rulings will be parallel, which gives cylindrical surfaces for the deformed unit cell. Of course, as can be seen from Figure 4, different unit cells have different cylindrical surfaces. We want to emphasize that the procedure outlined here gives one simple way to make helical origami structures with curved tiles, but the more general procedure described at the beginning of this section gives other possibilities.

In the implementation, if the planar crease $\mathbf{y}_1(s)$ and the constant ruling \mathbf{t}_1 of one tile are given, the ruling of the other tile will be found by $\mathbf{t}_2 = -\mathbf{P}_1\mathbf{t}_1$. Since $\mathbf{y}_0(s)$ is a planar curve in the tile, a simple way to get $\mathbf{y}_0(s)$ is to cut off the rulings with a plane, whose normal vector will be the binormal \mathbf{b}_0 of $\mathbf{y}_0(s)$. Once \mathbf{y}_0 is found, \mathbf{y}_2 will be determined since $\mathbf{b}_2 = -\mathbf{P}_1\mathbf{b}_0$ from (77). Specifically, the two boundaries $\mathbf{y}_0(s)$ and $\mathbf{y}_2(s)$ can be obtained by

$$\mathbf{y}_0 = \mathbf{y}_1 - \frac{(\mathbf{y}_1 - \mathbf{y}_1(s_1)) \cdot \mathbf{b}_0}{\mathbf{t}_1 \cdot \mathbf{b}_0} \mathbf{t}_1, \quad \mathbf{y}_2 = \mathbf{y}_1 + \frac{(\mathbf{y}_1 - \mathbf{y}_1(s_2)) \cdot \mathbf{b}_0}{\mathbf{t}_1 \cdot \mathbf{b}_0} \mathbf{t}_2. \quad (78)$$

The creases \mathbf{y}_0 and \mathbf{y}_2 given by (78) have the same configuration since (77) is satisfied. Also, $\mathbf{x}'_0 = \mathbf{x}'_2$ will be automatically satisfied in the reference domain, which can be verified by using $\mathbf{x}'_0 = \mathbf{F}_1^T\mathbf{y}'_0$ and $\mathbf{x}'_2 = \mathbf{F}_2^T\mathbf{y}'_2$ and Corollary 3.3. Therefore, the adjacent unit cells will be compatible at curved creases in both reference and deformed domains after group operations. An algorithm to construct the helical curved origami follows.

Algorithm 1 Helical group

Input: planar crease $\mathbf{y}_1(s)$, constant binormal \mathbf{b}_0 , constant ruling \mathbf{t}_1 of one surface.

Output: helical curved origami.

Steps:

1: Find the unit cell \mathcal{S} :

- Find the deformed rulings of the second surface:

$$\mathbf{t}_2 = -\mathbf{P}_1\mathbf{t}_1. \quad (79)$$

- Find the two boundary creases $\mathbf{y}_0(s)$ and $\mathbf{y}_2(s)$:

$$\mathbf{y}_0(s) = \mathbf{y}_1(s) - \frac{(\mathbf{y}_1(s) - \mathbf{y}_1(s_1)) \cdot \mathbf{b}_0}{\mathbf{t}_1 \cdot \mathbf{b}_0} \mathbf{t}_1, \quad (80)$$

$$\mathbf{y}_2(s) = \mathbf{y}_1(s) + \frac{(\mathbf{y}_1(s) - \mathbf{y}_1(s_2)) \cdot \mathbf{b}_0}{\mathbf{t}_1 \cdot \mathbf{b}_0} \mathbf{t}_2, \quad (81)$$

- Construct the deformed unit cell:

$$\mathcal{S} = \left\{ \begin{array}{l} (1-v)\mathbf{y}_1(s) + v\mathbf{y}_0(s) \\ (1-v)\mathbf{y}_1(s) + v\mathbf{y}_2(s) \end{array} : 0 < v < 1, s_1 < s < s_2 \right\} \quad (82)$$

- 2: Find the group parameters of \mathcal{G} :

$$\mathbf{e}_R = \frac{\mathbf{b}_0 \times \mathbf{b}_1}{|\mathbf{b}_0 \times \mathbf{b}_1|} \quad (83)$$

$$\theta_1 = \text{sign}(\mathbf{e}_R \cdot (\mathbf{y}_a - \mathbf{y}_b) \times (\mathbf{y}_d - \mathbf{y}_c)) \arccos \left(\frac{\mathbf{A}(\mathbf{y}_a - \mathbf{y}_b) \cdot \mathbf{A}(\mathbf{y}_d - \mathbf{y}_c)}{|\mathbf{y}_a - \mathbf{y}_b| |\mathbf{y}_d - \mathbf{y}_c|} \right) \quad (84)$$

$$\theta_2 = \text{sign}(\mathbf{e}_R \cdot (\mathbf{y}_a - \mathbf{y}_d) \times (\mathbf{y}_b - \mathbf{y}_c)) \arccos \left(\frac{\mathbf{A}(\mathbf{y}_a - \mathbf{y}_d) \cdot \mathbf{A}(\mathbf{y}_b - \mathbf{y}_c)}{|\mathbf{y}_a - \mathbf{y}_d| |\mathbf{y}_b - \mathbf{y}_c|} \right) \quad (85)$$

$$\tau_1 = \mathbf{e}_R \cdot (\mathbf{y}_a - \mathbf{y}_d) \quad (86)$$

$$\tau_2 = \mathbf{e}_R \cdot (\mathbf{y}_a - \mathbf{y}_b) \quad (87)$$

$$\mathbf{z} = \bar{\mathbf{R}}_2 \mathbf{A}(\mathbf{y}_a - \mathbf{R}_2 \mathbf{y}_d) \quad (88)$$

where $\mathbf{A} = \mathbf{I} - \mathbf{e}_R \otimes \mathbf{e}_R$, $\bar{\mathbf{R}}_2 = (\mathbf{I} + \mathbf{e}_R \otimes \mathbf{e}_R - \mathbf{R}_2)^{-1} - \mathbf{e}_R \otimes \mathbf{e}_R$, $\mathbf{y}_a = \mathbf{y}_2(s_1)$, $\mathbf{y}_b = \mathbf{y}_0(s_1)$, and $\mathbf{y}_c = \mathbf{y}_0(s_2)$, $\mathbf{y}_d = \mathbf{y}_2(s_2)$.

- 3: Apply the helical group to the unit cell:

$$\mathcal{G}(\mathcal{S}) = \{g_1^p g_2^q(\mathcal{S}) : (p, q) \in \mathbb{Z}^2\}. \quad (89)$$

Here if $\mathbf{y}_1(s)$ is fixed, the group parameters (83-88) will rely on \mathbf{b}_0 and \mathbf{t}_1 . In this algorithm, to get a globally compatible helical origami, suitable \mathbf{b}_0 and \mathbf{t}_1 are chosen in advance by numerically solving (71) with certain (p^*, q^*) by plugging in the group parameters with respect to \mathbf{b}_0 and \mathbf{t} . See some helical curved tile origami in Figure 4.

4.2 Circle groups

In this subsection, we study the degenerate case where a circle group is applied to a partially folded unit cell as shown in Figure 5. The reference unit cell in this case consists of two parallelogram-like planar sheets. The whole reference domain can be obtained by taking the product of a translation to Ω . To define this translation, let

$$t = (\mathbf{I}|\mathbf{c}). \quad (90)$$

Then the overall flat tessellation in Figure 5(b) is obtained by

$$\mathcal{T}(\Omega) = \{t^p(\Omega), p \in \mathbb{Z}\}. \quad (91)$$

For the deformed domain define

$$g = (\mathbf{R}|(\mathbf{I} - \mathbf{R})\mathbf{z}), \quad (92)$$

where \mathbf{R} is a rotation of angle $2\pi/n$ with $n \in \mathbb{Z}$, $\mathbf{z} \in \mathbb{R}^3$ and $\mathbf{z} \cdot \mathbf{e}_R = 0$, \mathbf{e}_R is the unit vector along the axis of \mathbf{R} . Then the overall deformed configuration is obtained by

$$\mathcal{G}(\mathcal{S}) = \{g^p(\mathcal{S}), p \in \mathbb{Z}\}. \quad (93)$$

By following the same steps in the helical origami, one can get the same conclusion that all the creases are planar curves and all surfaces are cylindrical surfaces. The algorithm to construct curved origami using a circle group follows.

Algorithm 2 Circle group

Input: planar crease $\mathbf{y}_1(s)$ and constant ruling \mathbf{t}_1 of one surface, the order of group \mathcal{G} : n .

Output: curved origami with rotational symmetry.

Steps:

1: Find the unit cell:

- Find the deformed rulings of the second surface:

$$\mathbf{t}_2 = -\mathbf{P}_1\mathbf{t}_1 \quad (94)$$

- Find the axis of \mathbf{R} and the two boundary creases $\mathbf{y}_0(s)$ and $\mathbf{y}_2(s)$:

$$\mathbf{e}_R = \frac{\mathbf{t}_1 \times \mathbf{t}_2}{|\mathbf{t}_1 \times \mathbf{t}_2|}, \quad (95)$$

$$\mathbf{y}_0(s) = \left(\mathbf{I} - \frac{\mathbf{t}_1 \otimes \mathbf{b}_0}{\mathbf{t}_1 \cdot \mathbf{b}_0}\right)\mathbf{y}_1(s) + a\mathbf{t}_1, \quad a \in \mathbb{R} \quad (96)$$

$$\mathbf{y}_2(s) = \left(\mathbf{I} - \frac{\mathbf{t}_2 \otimes \mathbf{b}_2}{\mathbf{t}_2 \cdot \mathbf{b}_2}\right)\mathbf{y}_1(s) + b\mathbf{t}_2, \quad b \in \mathbb{R} \quad (97)$$

where $\mathbf{b}_0 = \mathbf{R}_\alpha \mathbf{b}_1$, $\mathbf{b}_2 = -\mathbf{P}_1 \mathbf{b}_0$ and \mathbf{R}_α is a rotation about axis \mathbf{e}_R with angle $\alpha = \frac{\pi}{2} - \frac{\pi}{n}$, $n \in \mathbb{Z}$.

- Construct the deformed unit cell:

$$\mathcal{S} = \left\{ \begin{array}{l} (1-v)\mathbf{y}_1(s) + v\mathbf{y}_0(s) \\ (1-v)\mathbf{y}_1(s) + v\mathbf{y}_2(s) \end{array} : 0 < v < 1, s_1 < s < s_2 \right\} \quad (98)$$

2: Find the group parameters of \mathcal{G} :

$$\mathbf{z} = \bar{\mathbf{R}}\mathbf{A}(\mathbf{y}_a - \mathbf{R}\mathbf{y}_d). \quad (99)$$

where $\mathbf{A} = \mathbf{I} - \mathbf{e}_R \otimes \mathbf{e}_R$, $\bar{\mathbf{R}} = (\mathbf{I} + \mathbf{e}_R \otimes \mathbf{e}_R - \mathbf{R})^{-1} - \mathbf{e}_R \otimes \mathbf{e}_R$.

3: Apply the circle group to the unit cell:

$$\mathcal{G}(\mathcal{S}) = \{g^p(\mathcal{S}), p \in \mathbb{Z}\}. \quad (100)$$

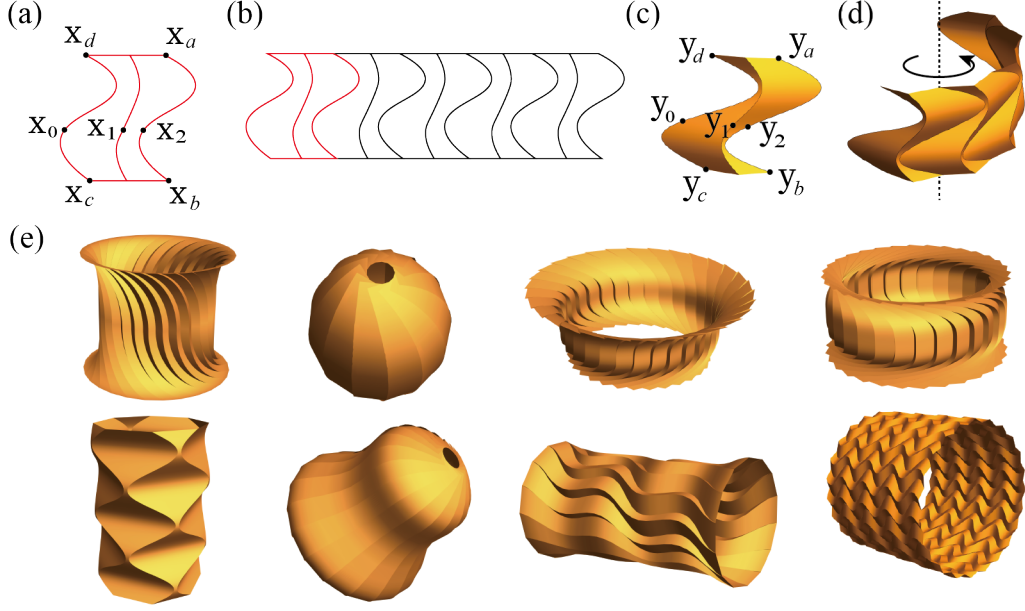


Figure 5: Curved tile origami generated by circle groups. (a) Reference unit cell. (b) Reference configuration. (c) Deformed unit cell. (d) Deformed configuration. (e) Some examples.

4.3 Translation groups

Periodic curved origami is obtained by applying translation groups to the unit cell \mathcal{S} . The schematics of the reference and deformed unit cells are shown in Figure 6. In the reference configuration, the crease $\mathbf{x}_2(s)$ is obtained by translating $\mathbf{x}_0(s)$ by a translation \mathbf{c}_1 . Similarly, in the deformed configuration, $\mathbf{y}_2(s)$ is obtained from $\mathbf{y}_0(s)$ by \mathbf{c}_2 . Define

$$t_1 = (\mathbf{I}|\mathbf{c}_1), \quad g_1 = (\mathbf{I}|\mathbf{c}_2), \quad (101)$$

then the whole reference domain and deformed domain are found by

$$\mathcal{T}(\Omega) = \{t_1^p(\Omega), p \in \mathbb{Z}\}, \quad \mathcal{G}(\mathcal{S}) = \{g_1^p(\mathcal{S}), p \in \mathbb{Z}\}. \quad (102)$$

Since $\mathbf{x}_2 = t_1(\mathbf{x}_0) = \mathbf{x}_0 + \mathbf{c}_1$ and $\mathbf{y}_2 = g_1(\mathbf{y}_0) = \mathbf{y}_0 + \mathbf{c}_2$, we have $\mathbf{x}'_0 = \mathbf{x}'_2$ and $\mathbf{y}'_0 = \mathbf{y}'_2$. Thus, $\mathbf{y}'_2 = \mathbf{F}_2\mathbf{x}'_2 = \mathbf{y}'_0 = \mathbf{F}_1\mathbf{x}'_0 = \mathbf{F}_1\mathbf{x}'_2$. At crease \mathbf{y}_1 , the compatibility condition gives $\mathbf{F}_1\mathbf{x}'_1 = \mathbf{F}_2\mathbf{x}'_1$. So

$$(\mathbf{F}_1 - \mathbf{F}_2)\mathbf{x}'_1 = 0, \quad (\mathbf{F}_1 - \mathbf{F}_2)\mathbf{x}'_2 = 0 \quad \text{with } \mathbf{F}_1 \neq \mathbf{F}_2. \quad (103)$$

We get $\mathbf{x}'_2 = c\mathbf{x}'_1, c \in \mathbb{R}$. Therefore, $\mathbf{y}'_2 = \mathbf{F}_2\mathbf{x}'_2 = c\mathbf{F}_2\mathbf{x}'_1 = c\mathbf{y}'_1$. Similarly, we have $\mathbf{y}'_1 = c\mathbf{y}'_0$. Then $\mathbf{y}'_2 = \mathbf{y}'_0$ implies $c = 1$. Thus,

$$\mathbf{y}'_0 = \mathbf{y}'_1 = \mathbf{y}'_2. \quad (104)$$

Let $\mathbf{y}_2 = \mathbf{y}_1 + v_1\mathbf{t}_1$ and $\mathbf{y}_2 = \mathbf{y}_1 + v_2\mathbf{t}_2$. Then $v_1\mathbf{t}_1$ and $v_2\mathbf{t}_2$ will be constant independent of s from (104). Therefore, the two surfaces in \mathcal{S} will be cylindrical surfaces, but the deformed creases are not necessarily planar curves in this case.

In the implementation, we get the cylindrical surfaces by assigning planar normal vectors \mathbf{n}_1 and \mathbf{n}_2 according to Corollary 3.4 and Corollary 3.5. The algorithm is given below.

Algorithm 3 Translation group

Input: the two planar normal vectors $\mathbf{n}_1(s), \mathbf{n}_2(s)$.

Output: periodic curved origami.

Steps:

1: Find the unit cell:

- Find the crease $\mathbf{y}_1(s)$:

$$\mathbf{y}_1(s) = \bar{\mathbf{y}}_1 + \int_{s_1}^s \frac{\mathbf{n}_1 \times \mathbf{n}_2}{|\mathbf{n}_1 \times \mathbf{n}_2|} dr. \quad (105)$$

where $\bar{\mathbf{y}}_1 = \mathbf{y}_1(s_1)$ is a given constant.

- Find the two constant rulings \mathbf{t}_1 and \mathbf{t}_2 :

$$\mathbf{t}_1 = \mathbf{n}_1 \times \frac{\mathbf{n}'_1}{|\mathbf{n}'_1|}, \quad \mathbf{t}_2 = \mathbf{n}_2 \times \frac{\mathbf{n}'_2}{|\mathbf{n}'_2|}. \quad (106)$$

- Find the two boundary creases $\mathbf{y}_0(s)$ and $\mathbf{y}_2(s)$:

$$\mathbf{y}_0(s) = \mathbf{y}_1(s) + v_1 \mathbf{t}_1, \quad (107)$$

$$\mathbf{y}_2(s) = \mathbf{y}_1(s) + v_2 \mathbf{t}_2, \quad (108)$$

where $v_1, v_2 > 0$ are constant.

- Construct the deformed unit cell:

$$\mathcal{S} = \left\{ \begin{array}{l} (1-v)\mathbf{y}_1(s) + v\mathbf{y}_0(s) \\ (1-v)\mathbf{y}_1(s) + v\mathbf{y}_2(s) \end{array} : 0 < v < 1, s_1 < s < s_2 \right\}. \quad (109)$$

2: Find the group parameters of \mathcal{G} :

$$\mathbf{c}_2 = \mathbf{y}_a - \mathbf{y}_d. \quad (110)$$

3: Apply the circle group to the unit cell:

$$\mathcal{G}(\mathcal{S}) = \{g^p(\mathcal{S}), p \in \mathbb{Z}\}. \quad (111)$$

Since the upper boundary $\widehat{\mathbf{x}_d \mathbf{x}_a}$ is a translation of the lower boundary $\widehat{\mathbf{x}_c \mathbf{x}_b}$ in Ω , we can also introduce the second translation generator to Ω : $t_2 = (\mathbf{I}|\mathbf{c}_3)$, where $\mathbf{c}_3 = \mathbf{x}_a - \mathbf{x}_b$. Then the reference domain is given by

$$\mathcal{T}(\Omega) = \{t_1^p t_2^q(\Omega), p, q \in \mathbb{Z}\}, \quad (112)$$

see Figure 6(a)₃. In the deformed domain, $\mathbf{y}(g_3(\Omega))$ is automatically compatible with $\mathbf{y}(\Omega)$. Let $\mathbf{c}_4 = \mathbf{y}_a - \mathbf{y}_b$ and $g_2 = (\mathbf{I}|\mathbf{c}_4)$, the whole deformed configuration is found by

$$\mathcal{G}(\mathcal{S}) = \{g_1^p g_2^q(\mathcal{S}), (p, q) \in \mathbb{Z}^2\}. \quad (113)$$

See examples in Figure 6(d).

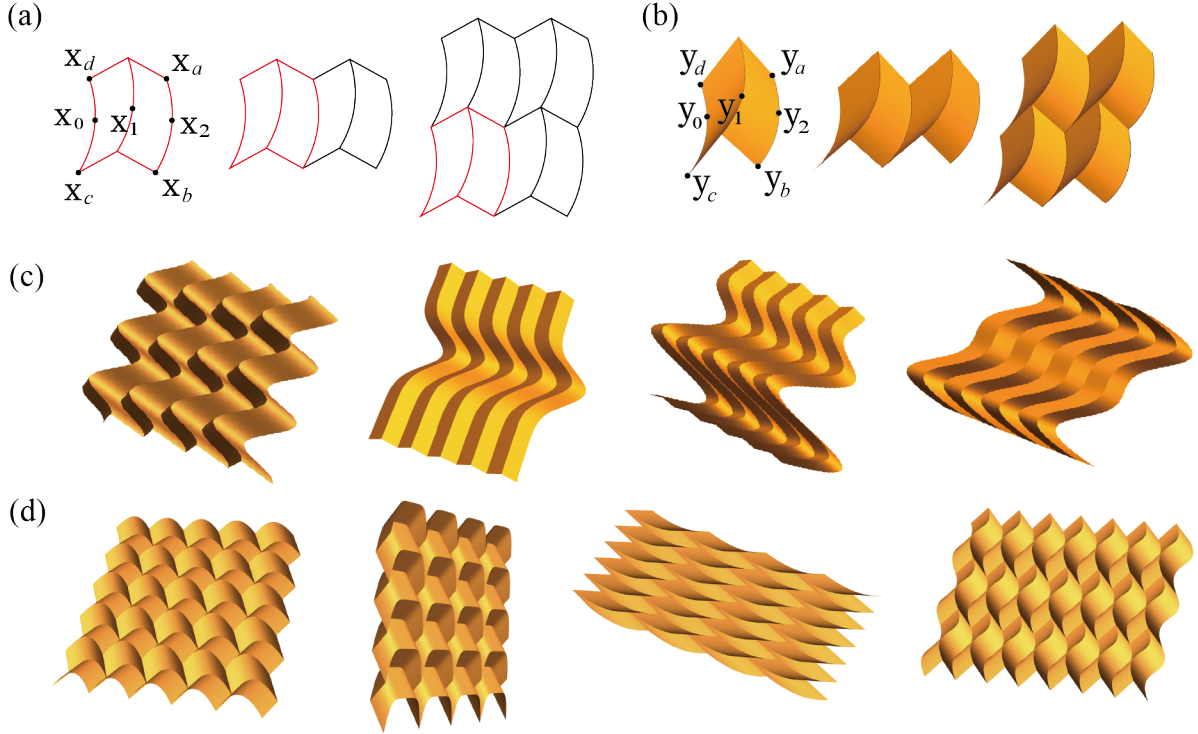


Figure 6: Curved tile origami generated by translation groups. (a) Reference configurations (flat). (b) Deformed configurations. (c) Some examples generated by the translation groups with one generator. (d) Some examples generated by the translation groups with two generators.

4.4 More on circle groups

As an alternative to the constructions of Section 4.2, in this subsection we apply circle groups to both the reference unit cell and the deformed unit cell, see Figure 7. Define

$$t = (\mathbf{R}_1 | \mathbf{0}), \quad g = (\mathbf{R}_2 | \mathbf{0}), \quad (114)$$

where $\mathbf{R}_1 \in \text{SO}(2)$ and $\mathbf{R}_2 \in \text{SO}(3)$. The reference and deformed domains are given by

$$\mathcal{T}(\Omega) = \{t^p(\Omega) : p \in \mathbb{Z}\}, \quad \mathcal{G}(\mathcal{S}) = \{g^p(\mathcal{S}) : p \in \mathbb{Z}\}. \quad (115)$$

Let the normal vectors of \mathcal{S}_1 and \mathcal{S}_2 on the both sides of $\mathbf{y}_1(s)$ be $\mathbf{n}_1(s)$ and $\mathbf{n}_2(s)$. Then the normal vectors on the both sides of $\mathbf{y}_2(s)$ will be $\mathbf{n}_2(s)$ and $\mathbf{R}_2 \mathbf{n}_1(s)$. Let $\mathbf{y}_1(s_1) = \mathbf{y}_2(s_1) = \mathbf{0}$. According to Corollary 3.4, an algorithm is presented in Algorithm 4.

Algorithm 4 Circle groups

Input: the normal vectors \mathbf{n}_1 and \mathbf{n}_2 , rotation \mathbf{R}_2 .

Output: periodic curved origami.

Steps:

1: Find the unit cell:

- Find the crease $\mathbf{y}_1(s)$:

$$\mathbf{y}_1(s) = \int_{s_1}^s \frac{\mathbf{n}_1 \times \mathbf{n}_2}{|\mathbf{n}_1 \times \mathbf{n}_2|} dr. \quad (116)$$

- Find the two boundary creases $\mathbf{y}_0(s)$ and $\mathbf{y}_2(s)$:

$$\mathbf{y}_2(s) = \int_{s_1}^s \frac{\mathbf{R}_2 \mathbf{n}_1 \times \mathbf{n}_2}{|\mathbf{R}_2 \mathbf{n}_1 \times \mathbf{n}_2|} dr, \quad (117)$$

$$\mathbf{y}_0(s) = \mathbf{R}_2^T \mathbf{y}_2(s). \quad (118)$$

- Construct the deformed unit cell:

$$\mathcal{S} = \left\{ \begin{array}{l} (1-v)\mathbf{y}_1(s) + v\mathbf{y}_0(s) \\ (1-v)\mathbf{y}_1(s) + v\mathbf{y}_2(s) \end{array} : 0 < v < 1, s_1 < s < s_2 \right\}. \quad (119)$$

2: Apply the circle group to the unit cell:

$$\mathcal{G}(\mathcal{S}) = \{g^p(\mathcal{S}), p \in \mathbb{Z}\}. \quad (120)$$

See some examples in Figure (7).

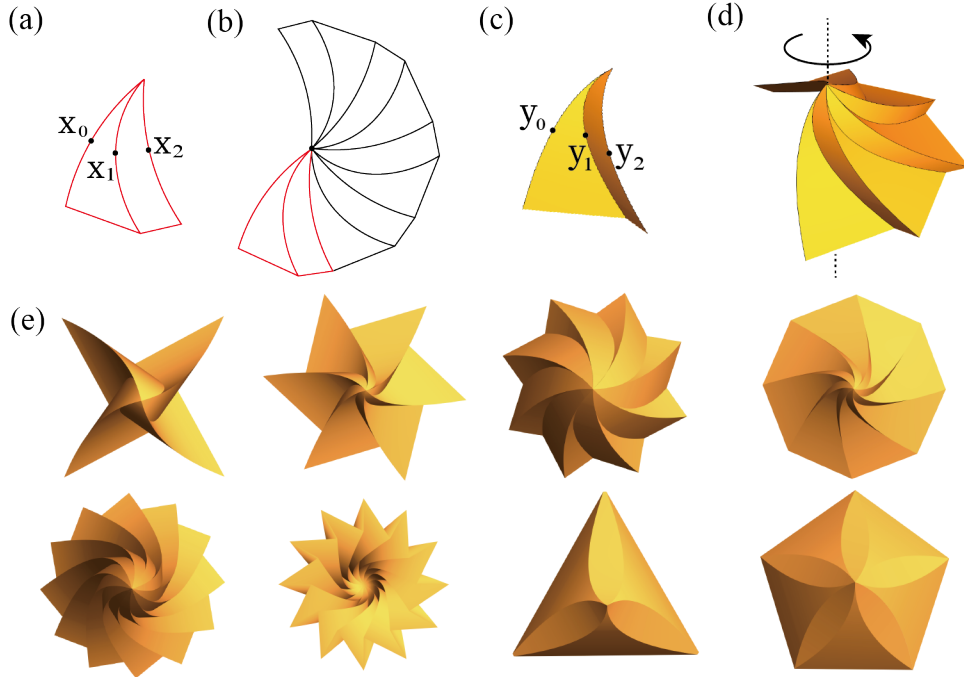


Figure 7: Curved tile origami generated by circle groups. (a) Reference unit cell. (b) Reference configuration. (c) Deformed unit cell. (d) Deformed configuration. (e) Some examples.

4.5 Conformal groups

Conformal groups, which include dilatations as well as rotations and translations, can be used to construct origami structures. At first, one might think that the dilatations present in conformal groups might be incompatible with the pure isometric deformations possible in thin tiles. However, one can simply recognize that the basic scaling law of nonlinear elasticity theory, $\mathbf{y}(\mathbf{x}, t) \rightarrow$

$\eta\mathbf{y}((1/\eta)\mathbf{x}, (1/\eta)t)$, which preserves the deformation gradient, stress, balance of linear momentum (no body force), isometric deformations, etc., can be invoked by simply allowing neighboring tiles to be related by the appropriate dilatation, as well as a possible rotation and translation. To be compatible with elasticity scaling, the same dilatation must be used on corresponding tiles in the reference and deformed domains. Conformal groups necessarily have at least one accumulation point, so this point must of course be avoided, by e.g., introducing a small cut-out.

Since neighboring tiles are related by dilatation, conformal groups feature structures that have a natural mechanism of growth, beginning from their accumulation points (Figure 8). In this regard our structures here are similar to some discussed by Thompson [14], especially the examples of sea shells and horns. While isometries do not play a significant role in his analysis, the group orbit procedure (described in words) applied with conformal groups is central to his work.

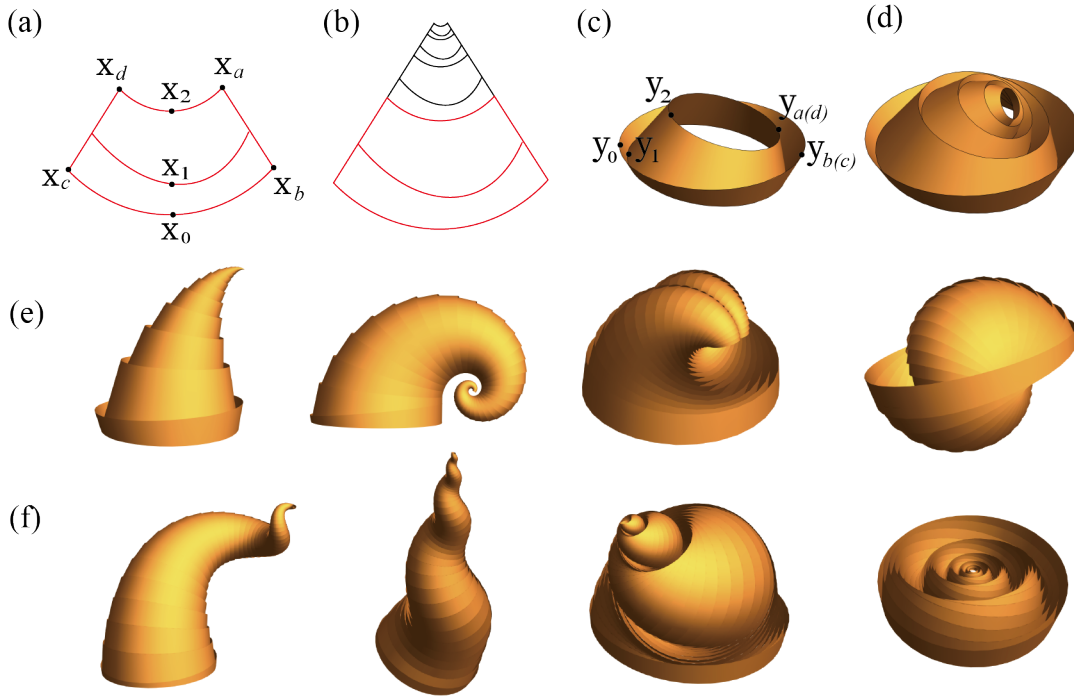


Figure 8: Curved tile origami generated by conformal groups. (a) Reference unit cell. (b) Reference configuration. (c) Deformed unit cell. (d) Deformed configuration. (e-f) Some examples.

We say that \mathcal{G} is a conformal Euclidean group if \mathcal{G} is a group of affine linear mappings of the form $g = (\eta\mathbf{Q}|\mathbf{c})$, where $\eta > 0$ and $\eta \neq 1$, $\mathbf{Q} \in \text{O}(3)$, $\mathbf{c} \in \mathbb{R}^3$. We will be particularly interested in the generators of the form

$$g_i = (\eta_i \mathbf{R}_{\theta_i} | (\mathbf{I} - \eta_i \mathbf{R}_{\theta_i}) \mathbf{c}_i), \quad (121)$$

where $\eta_i > 0$ and $\eta_i \neq 1$, $\mathbf{R}_{\theta_i} \in \text{SO}(3)$ denotes a rotation of angle θ_i , $\mathbf{c}_i \in \mathbb{R}^3$. Let the generators for the reference domain and deformed domain be t and g respectively, which are defined by

$$t = (\eta \mathbf{I} | (1 - \eta) \mathbf{c}_0), \quad g = (\eta \mathbf{R} | (\mathbf{I} - \eta \mathbf{R}) \mathbf{c}). \quad (122)$$

The reference unit cell Ω is shown in Figure 8(a). The whole reference domain can be obtained by

$$\mathcal{T}(\Omega) = \{t^p(\Omega) : p \in \mathbb{Z}\}, \quad (123)$$

where $t^p = (\eta^p \mathbf{I} | (1 - \eta^p) \mathbf{c}_0)$. The deformed unit cell \mathcal{S} is shown in Figure 8(c), and the deformed configuration in Figure 8(d) is obtained by

$$\mathcal{G}(\mathcal{S}) = \{g^p(\mathcal{S}) : p \in \mathbb{Z}\}, \quad (124)$$

where $g^p = (\eta^p \mathbf{R}_{p\theta} | (\mathbf{I} - \eta^p \mathbf{R}_{p\theta}) \mathbf{c})$ and the subscript denotes the rotational angle of \mathbf{R} . Since $\mathbf{x}_2 = t(\mathbf{x}_0) = \eta \mathbf{x}_0 + (1 - \eta) \mathbf{c}_0$ and $\mathbf{y}_2 = g(\mathbf{y}_0) = \eta \mathbf{R} \mathbf{y}_0 + (\mathbf{I} - \eta \mathbf{R}) \mathbf{c}$, we have

$$\mathbf{x}'_2 = \eta \mathbf{x}'_0, \quad \mathbf{y}'_2 = \eta \mathbf{R} \mathbf{y}'_0 \quad (125)$$

Combining this with $\mathbf{y}'_0 = \mathbf{F}_1 \mathbf{x}'_0$ and $\mathbf{y}'_2 = \mathbf{F}_2 \mathbf{x}'_2$, we get $\mathbf{y}'_2 = \mathbf{R} \mathbf{F}_1 \mathbf{x}'_2 = \mathbf{F}_2 \mathbf{x}'_2$. This gives the compatibility condition at $\mathbf{x}_2(s)$. Because $\mathbf{F}_2 = \mathbf{P}_1 \mathbf{F}_1$, $\mathbf{R} \mathbf{F}_1 = \mathbf{P}_2 \mathbf{F}_2$, we have $\mathbf{F}_1 = \mathbf{P}_1 \mathbf{P}_2 \mathbf{R} \mathbf{F}_1$. Notice that $\mathbf{P}_1 \mathbf{P}_2 \mathbf{R} \in \text{SO}(3)$. We get $\mathbf{P}_1 \mathbf{P}_2 \mathbf{R} = \mathbf{I}$ and therefore $\mathbf{P}_2 \mathbf{P}_1 = \mathbf{R}$. We obtain the same conclusion that the creases are planar curves as discussed in Section 4.1. Thus, the rulings in the reference domain with same s are collinear. Since $\eta \neq 1$, the extension of all reference rulings, which can be given by $\mathbf{x}_2 - \mathbf{x}_0$, will intersect at a common point because of the proportional relationship of $\mathbf{x}'_2 = \eta \mathbf{x}'_0$. Therefore, the deformed surfaces are generalized conical surfaces. Algorithm 5 is used to construct conformal curved origami.

Algorithm 5 Conformal group

Input: two planar creases on the conical surface: $\mathbf{y}_0(s)$ and $\mathbf{y}_1(s)$.

Output: conformal curved origami.

Steps:

1: Find the unit cell:

- Find the deformed rulings:

$$\mathbf{t}_1(s) = \frac{\mathbf{y}_0(s) - \mathbf{y}_1(s)}{|\mathbf{y}_0(s) - \mathbf{y}_1(s)|}, \quad \mathbf{t}_2(s) = -\mathbf{P}_1 \mathbf{t}_1(s). \quad (126)$$

- Find the crease $\mathbf{y}_2(s)$:

$$\mathbf{y}_2(s) = \left(\mathbf{I} - \frac{\mathbf{t}_2(s) \otimes \mathbf{b}_2}{\mathbf{t}_2(s) \cdot \mathbf{b}_2} \right) \mathbf{y}_1(s) + b \mathbf{t}_2(s), \quad (127)$$

where $b \in \mathbb{R}$ and $\mathbf{b}_2 = -\mathbf{P}_1 \mathbf{b}_0$.

- Construct the deformed unit cell:

$$\mathcal{S} = \left\{ \begin{array}{l} (1-v)\mathbf{y}_1(s) + v\mathbf{y}_0(s) \\ (1-v)\mathbf{y}_1(s) + v\mathbf{y}_2(s) \end{array} : 0 < v < 1, s_1 < s < s_2 \right\} \quad (128)$$

2: Find the group parameters of \mathcal{G} :

$$\eta = \frac{|\mathbf{y}_2 - \mathbf{y}_b|}{|\mathbf{y}_0 - \mathbf{y}_a|} \quad (129)$$

$$\mathbf{e}_R = \frac{\tilde{\mathbf{e}}_R}{|\tilde{\mathbf{e}}_R|}, \quad \tilde{\mathbf{e}}_R = \left(\frac{\mathbf{y}_0 - \mathbf{y}_a}{|\mathbf{y}_0 - \mathbf{y}_a|} - \frac{\mathbf{y}_2 - \mathbf{y}_b}{|\mathbf{y}_2 - \mathbf{y}_b|} \right) \times \left(\frac{\mathbf{y}_0 - \mathbf{y}_2}{|\mathbf{y}_0 - \mathbf{y}_2|} - \frac{\mathbf{y}_a - \mathbf{y}_b}{|\mathbf{y}_a - \mathbf{y}_b|} \right) \quad (130)$$

$$\theta = \text{sign}(\mathbf{e} \cdot (\mathbf{y}_0 - \mathbf{y}_a) \times (\mathbf{y}_2 - \mathbf{y}_b)) \arccos \left(\frac{\mathbf{A}(\mathbf{y}_0 - \mathbf{y}_a) \cdot \mathbf{A}(\mathbf{y}_2 - \mathbf{y}_b)}{|\mathbf{A}(\mathbf{y}_0 - \mathbf{y}_a)| |\mathbf{A}(\mathbf{y}_2 - \mathbf{y}_b)|} \right) \quad (131)$$

$$\mathbf{c} = (\mathbf{I} - \eta \mathbf{R})^{-1} (-\eta \mathbf{R} \mathbf{y}_0 + \mathbf{y}_2) \quad (132)$$

where \mathbf{e}_R is the axis of \mathbf{R} and $\mathbf{A} = \mathbf{I} - \mathbf{e}_R \otimes \mathbf{e}_R$.

3: Apply the circle group to the unit cell:

$$\mathcal{G}(\mathcal{S}) = \{g^p(\mathcal{S}), p \in \mathbb{Z}\}. \quad (133)$$

Thus, applying the group \mathcal{G} with the group parameters listed above to the unit cell, we can get conformal origami structures. Some examples are shown in Figure 8(e-f).

5 Curved tile generalizations of the Miura pattern

When folding a piece of paper in a random way, it is commonly observed that several creases intersect at one point. In this section, we study the kinematics of curved tiles in this situation and discuss one special case where the rulings of adjacent tiles intersect at creases and form closed loops around the vertex, that is, all creases can be parameterized by one parameter s . A necessary and sufficient condition for constructing such compatible curved origami is given below.

Theorem 5.1. *Consider an origami structure with n ($n > 2$) curved creases intersecting at one vertex. Suppose the reference rulings form closed loops around the vertex in the reference domain. Denote deformed creases counterclockwise to be $\mathbf{y}_i(s)$, $0 < s < s_1$, $i = 1, \dots, n$. The points of $\mathbf{y}_i(s)$, $i = 1, \dots, n$ with the same s are connected by straight deformed rulings. Assume the conditions and definitions of Theorem 3.1 on $\mathbf{y}_i(s)$. Let $\mathbf{b}_i(s)$ be the binormal vector of the i^{th} crease at $\mathbf{y}_i(s)$, and let $\mathbf{P}_i(s) = \mathbf{I} - 2\mathbf{b}_i(s) \otimes \mathbf{b}_i(s)$. Then a necessary and sufficient condition for getting a compatible curved origami is*

$$\mathbf{P}_1(s)\mathbf{P}_2(s) \dots \mathbf{P}_{n-1}(s)\mathbf{P}_n(s) = \mathbf{I}, \quad n \text{ is even.} \quad (134)$$

See proof in A.1. As $n = 4$, we obtain the generalized Miura origami. Let the preimage of $\mathbf{y}_i(s)$ be $\mathbf{x}_i(s)$, $i = 1, 2, 3, 4$, $0 < s < s_1$. Then the points $\mathbf{x}_1(s), \mathbf{x}_2(s), \mathbf{x}_3(s), \mathbf{x}_4(s)$ with same s will lie in the same loop. Figure 9(a) illustrates the reference configuration of four-fold curved origami, where the gray lines represent the reference rulings. According to Corollary 3.4, if adjacent normal vectors on both sides of each deformed crease satisfy (64), the origami at each crease is developable and the compatibility condition (134) is automatically satisfied, see also A.1. Based on the assumptions in Corollary 3.4, one algorithm to construct curved Miura origami with four creases is shown in Algorithm 6.

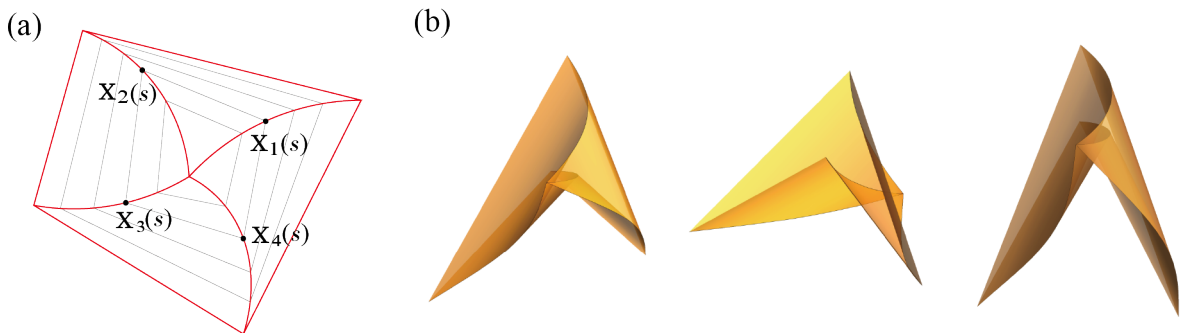


Figure 9: Curved Miura origami. (a) Schematic of reference configuration, where the gray lines represent the reference rulings. (b) Some examples.

Algorithm 6 Curved origami with multiple creases

Input: normal vectors $\mathbf{n}_1(s), \mathbf{n}_2(s), \mathbf{n}_3(s), \mathbf{n}_4(s)$.

Output: curved origami with multiple creases.

Steps:

1: Find the deformed creases: $\mathbf{y}_1(s), \mathbf{y}_2(s), \mathbf{y}_3(s), \mathbf{y}_4(s)$:

$$\mathbf{y}_1(s) = \int_0^s c_1 \frac{\mathbf{n}_1 \times \mathbf{n}_2}{|\mathbf{n}_1 \times \mathbf{n}_2|} dr, \quad \mathbf{y}_2(s) = \int_0^s c_2 \frac{\mathbf{n}_2 \times \mathbf{n}_3}{|\mathbf{n}_2 \times \mathbf{n}_3|} dr, \quad (135)$$

$$\mathbf{y}_3(s) = \int_0^s c_3 \frac{\mathbf{n}_3 \times \mathbf{n}_4}{|\mathbf{n}_3 \times \mathbf{n}_4|} dr, \quad \mathbf{y}_4(s) = \int_0^s c_4 \frac{\mathbf{n}_4 \times \mathbf{n}_1}{|\mathbf{n}_4 \times \mathbf{n}_1|} dr. \quad (136)$$

where $\mathbf{y}_i(0) = 0$ and $c_i \in C^1(0, s_1)$, $i = 1, 2, 3, 4$.

2: Construct the curved origami:

$$\mathcal{S} = \left\{ \begin{array}{l} (1-v)\mathbf{y}_1(s) + v\mathbf{y}_2(s) \\ (1-v)\mathbf{y}_2(s) + v\mathbf{y}_3(s) \\ (1-v)\mathbf{y}_3(s) + v\mathbf{y}_4(s) \\ (1-v)\mathbf{y}_4(s) + v\mathbf{y}_1(s) \end{array} : 0 < v < 1, 0 < s < s_2 \right\} \quad (137)$$

Figure 9(b) shows some examples of curved Miura origami in the folded state.

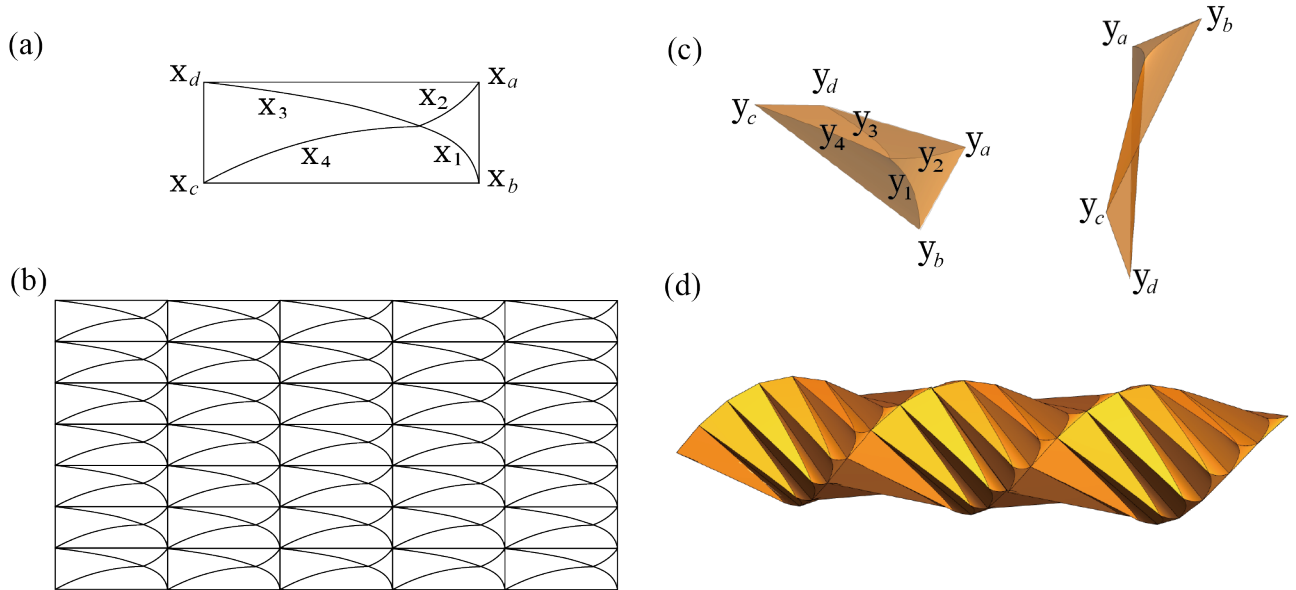


Figure 10: Helical origami with four curved creases in the unit cell. (a) Reference unit cell. (b) Reference configuration. (c) Deformed unit cell in different viewpoints. (d) Deformed configuration.

The group orbit procedure can also be applied to the generalized Miura pattern to design complex curved origami. Figure 10 shows an example in which the reference unit cell is a rectangle. We apply the translation group to the reference unit cell (Figure 10(a)) and the helical group to the

deformed unit cell (Figure 10(b)), as the examples shown in Section 4.1. In Figure 10, $\mathbf{y}_{1,2,3,4}$ are the images of the reference creases $\mathbf{x}_{1,2,3,4}$. Since isometric mappings always shorten distances, the mountain-valley assignments of the creases in this generalized Miura pattern will be 3 mountains–1 valley or 3 valleys–1 mountain, which are the same as that of the traditional Miura pattern, one can get the idea by linearization. In this example, creases $\mathbf{y}_1, \mathbf{y}_2, \mathbf{y}_4$ are mountains and crease \mathbf{y}_3 is a valley. The details of the group orbit procedure will not be repeated here.

6 Energy of curved tiles

6.1 Kirchhoff's nonlinear plate theory

The energy of an isometrically deformed surface can be accurately found by Kirchhoff's nonlinear plate theory. For an isometric mapping $\hat{\mathbf{y}} : \Omega \subset \mathbb{R}^2 \rightarrow \mathcal{S} \subset \mathbb{R}^3$, the energy is [23]

$$\mathcal{E}_s = \frac{h^3}{24} \int_{\Omega} 2\mu |\mathbb{I}|^2 + \frac{\lambda\mu}{\mu + \lambda/2} (\text{tr } \mathbb{I})^2 d\mathbf{x}, \quad (138)$$

where h is the thickness of Ω , $\mathbb{I} = \mathbf{n} \cdot \nabla \mathbf{F} = -\mathbf{F}^T \nabla \mathbf{n}$ is the second fundamental form, \mathbf{n} is the normal vector of the surface, λ, μ are the Lamé moduli. Substituting (11), the second fundamental form becomes

$$\mathbb{I} = \Lambda \mathbf{e}^{\perp} \otimes \mathbf{e}^{\perp}. \quad (139)$$

Thus, (138) can be further simplified to

$$\mathcal{E}_s = \frac{Eh^3}{24} \int_{\Omega} \Lambda^2 d\mathbf{x}, \quad (140)$$

where $E = 2\mu + \frac{\lambda\mu}{\mu + \lambda/2}$ is the plate modulus. The reference configuration Ω can be parameterized as $\mathbf{x}(s, v) = v\mathbf{e}(s) + \mathbf{x}_0(s)$, $s_1 < s < s_2$, $v_1(s) < v < v_2(s)$ by (16). So we can get

$$\mathcal{E}_s = \frac{Eh^3}{24} \int_{s_1}^{s_2} \int_{v_1}^{v_2} \Lambda^2 J dv ds, \quad (141)$$

where the Jacobian determinant J is

$$J = \frac{\partial \mathbf{x}(x_1, x_2)}{\partial \mathbf{x}(s, v)} = \det \begin{pmatrix} \mathbf{x}' \cdot \hat{\mathbf{e}}_1 & \mathbf{e} \cdot \hat{\mathbf{e}}_1 \\ \mathbf{x}' \cdot \hat{\mathbf{e}}_2 & \mathbf{e} \cdot \hat{\mathbf{e}}_2 \end{pmatrix} = \mathbf{x}' \cdot \mathbf{e}^{\perp}, \quad (142)$$

and $(\hat{\mathbf{e}}_1, \hat{\mathbf{e}}_2)$ is a fixed orthonormal basis with associated coordinates (x_1, x_2) . Since $\mathbf{n}' = \nabla \mathbf{n} \cdot \mathbf{x}'$ and $\mathbb{I} = -\mathbf{F}^T \nabla \mathbf{n}$, we get

$$\Lambda^2 = \frac{|\mathbf{n}'|^2}{(\mathbf{x}' \cdot \mathbf{e}^{\perp})^2}. \quad (143)$$

Thus, the energy \mathcal{E}_s is

$$\mathcal{E}_s = \frac{Eh^3}{24} \int_{s_1}^{s_2} \int_{v_1}^{v_2} \frac{|\mathbf{n}'|^2}{\mathbf{x}' \cdot \mathbf{e}^{\perp}} dv ds. \quad (144)$$

Then substituting $\mathbf{x}' = \mathbf{x}'_0 + v\mathbf{e}'$, we get

$$\mathcal{E}_s = \begin{cases} \frac{Eh^3}{24} \int_{s_1}^{s_2} \frac{|\mathbf{n}'|^2}{\mathbf{e}' \cdot \mathbf{e}^\perp} \log\left(\frac{\mathbf{x}'_0 \cdot \mathbf{e}^\perp + v_2 \mathbf{e}' \cdot \mathbf{e}^\perp}{\mathbf{x}'_0 \cdot \mathbf{e}^\perp + v_1 \mathbf{e}' \cdot \mathbf{e}^\perp}\right) ds, & \mathbf{e}' \neq 0, \\ \frac{Eh^3}{24} \int_{s_1}^{s_2} \frac{|\mathbf{n}'|^2}{\mathbf{x}'_0 \cdot \mathbf{e}^\perp} (v_2 - v_1) ds, & \mathbf{e}' = 0. \end{cases} \quad (145)$$

For a curved origami structure, $\mathbf{x}_0(s)$ is the reference crease and for each tile, we have $0 < v < \tilde{v}(s)$, where $\tilde{v}(s)$ is the length of the reference ruling at position s . Then the energy of each tile can be given by

$$\mathcal{E}_s = \begin{cases} \frac{Eh^3}{24} \int_{s_1}^{s_2} \frac{|\mathbf{n}'|^2}{\mathbf{e}' \cdot \mathbf{e}^\perp} \log\left(\frac{\mathbf{e}' \cdot \mathbf{e}^\perp}{\mathbf{x}'_0 \cdot \mathbf{e}^\perp} \tilde{v} + 1\right) ds, & \mathbf{e}' \neq 0, \\ \frac{Eh^3}{24} \int_{s_1}^{s_2} \frac{|\mathbf{n}'|^2 \tilde{v}}{\mathbf{x}'_0 \cdot \mathbf{e}^\perp} ds, & \mathbf{e}' = 0. \end{cases} \quad (146)$$

We also discuss the energy of the case where $\mathbf{x}'_0 \cdot \mathbf{e}^\perp = 0$, i.e., the surface is a tangent surface, see details in A.2.

In summary, for curved tile origami, the elastic energy according to Kirchhoff theory written using the parameterization given in this paper can be expressed as a simple, explicit 1-dimensional integral.

6.2 Discussion of the folding motion and the energy landscape

In this section, we discuss one strategy to get folding motions of curved origami. Different from rigid-foldable origami whose creases and tiles undergo rigid-body motions [1], curved origami with flexible creases and tiles exhibits infinite degrees of freedom of deformation during folding. One way to get a folding motion of curved origami is to prescribe the deformation process of its creases. Based on Theorem 3.1, if the reference crease and the deformed crease are given, the deformed configuration of curved origami will be determined. By designing the deformation process of the crease from \mathbf{x}_0 to \mathbf{y}_0 and ensuring the crease at each intermediate state satisfy the assumptions in the theorem, one will find the origami structure at each step and therefore get a folding motion.

Here is an example to show the strategy. As shown in Figure 11(a), the reference crease $\mathbf{x}_0(s)$, the deformed crease $\mathbf{y}_0(s)$ and the two reference regions Ω_1, Ω_2 on the opposite sides of $\mathbf{x}_0(s)$ are given by

$$\mathbf{x}_0(s) = \cos s \mathbf{e}_1 + \sin s \mathbf{e}_2, \quad s \in (0, \pi/2), \quad (147)$$

$$\mathbf{y}_0(s) = (\cos 2s \mathbf{e}_1 + \sin 2s \mathbf{e}_2)/2, \quad s \in (0, \pi/2), \quad (148)$$

$$\Omega_1 = \{r \cos s \mathbf{e}_1 + r \sin s \mathbf{e}_2 : s \in (0, \pi/2), r \in (1, 3/2)\}, \quad (149)$$

$$\Omega_2 = \{r \cos s \mathbf{e}_1 + r \sin s \mathbf{e}_2 : s \in (0, \pi/2), r \in (1/2, 1)\}. \quad (150)$$

Since a curve can be uniquely defined by its curvature and torsion [24], we use the curvature κ and torsion τ to parameterize the crease during folding. Let $\kappa_t(s)$ and $\tau_t(s)$ denote the curvature and torsion of the crease at arc length $s \in (s_1, s_2)$ at time $t \in [0, 1]$ respectively, where $t = 0$ represents the reference state and $t = 1$ represents the final state. Then in this example,

$$\kappa_0(s) = |\mathbf{x}_0''| = 1, \quad \kappa_1(s) = |\mathbf{y}_0''| = 2, \quad \tau_0(s) = \tau_1(s) = 0. \quad (151)$$

To simplify the problem, we assume κ and τ are independent of s during folding. The crease at time t can be expressed as

$$\mathbf{y}_0^t(s) = \frac{\kappa_t}{\omega_t^2} \cos(\omega_t s) \hat{\mathbf{e}}_1 + \frac{\kappa_t}{\omega_t^2} \sin(\omega_t s) \hat{\mathbf{e}}_2 + \frac{\tau_t s}{\omega_t} \hat{\mathbf{e}}_3, \quad s_1 < s < s_2 \quad (152)$$

where $\omega_t = \sqrt{\kappa_t^2 + \tau_t^2}$ and $\kappa_t \geq 1$, $(\hat{\mathbf{e}}_1, \hat{\mathbf{e}}_2, \hat{\mathbf{e}}_3)$ is a fixed orthonormal basis in \mathbb{R}^3 . By continuously changing κ_t and τ_t from $(\kappa_0, \tau_0) = (1, 0)$ to $(\kappa_1, \tau_1) = (2, 0)$, one will get deformation process of the crease and the associated folding motion the whole origami structure. Two folding motions are shown in Figure 11(d), the corresponding curvature and torsion in paths 1 and 2 are

$$\begin{cases} \kappa_t = t + 1, \\ \tau_t = 0, \end{cases} \quad \text{and} \quad \begin{cases} \kappa_t = t + 1, \\ \tau_t = 7t^2(t - 1)^2. \end{cases} \quad (153)$$

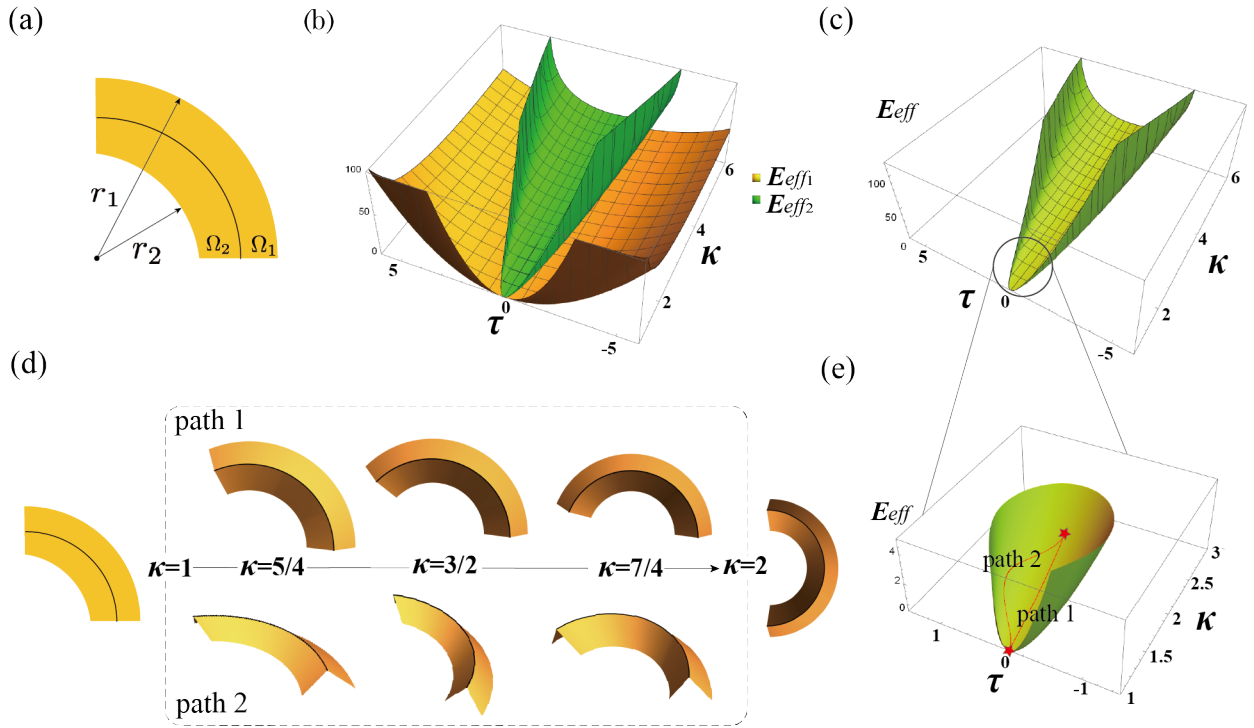


Figure 11: An example to show the folding process of curved tile origami. (a) The reference domain. (b) The energy landscapes of the two surfaces. (c) The total energy stored in the curved origami. (d) Two folding motions. (e) The corresponding energy paths of the two folding motions of (d).

The energy of the two tiles \mathcal{E}_{s_1} and \mathcal{E}_{s_2} in terms of curvature and torsion can be found by using Kirchhoff's nonlinear plate theory in (146), which is

$$\mathcal{E} = \mathcal{E}_{s_1} + \mathcal{E}_{s_2} = \frac{\pi E h^3}{48} E_{eff}, \quad (154)$$

where

$$E_{eff} = E_{eff1} + E_{eff2} = \frac{1}{2}(\kappa^2 + \tau^2 - 1) \log \frac{r_1^2(\kappa^2 + \tau^2 - 1) - \tau^2}{r_2^2(\kappa^2 + \tau^2 - 1) - \tau^2} \quad (155)$$

and E_{eff_1}, E_{eff_2} are the effective energy of $\mathcal{S}_1, \mathcal{S}_2$. Here we drop the subscript t in (155) and in Figure 11. The energy landscapes of E_{eff_1}, E_{eff_2} and E_{eff} are shown in Figure 11(b-c). The two red stars in Figure 11(e) correspond to the reference state and the final deformed state, and the two folding motions are highlighted by red lines. Without considering the intersection between \mathcal{S}_1 and \mathcal{S}_2 , each point in the energy surface in Figure 11(c) will be a physical folding state, and therefore any C^0 curve in the energy surface of E_{eff} will correspond to a folding motion.

From above example, the folding motions of curved origami with one crease can be obtained by designing the deformation process of its crease. For origami structures shown in Section 4, by specifying a suitable deformation process of the crease in the unit cell, group orbit procedure is potentially applied to the unit cell at each intermediate state, and then we will get a folding motion of the whole origami structure. Figure 12 shows three examples of folding motions in which helical groups, circle groups and translation groups are applied respectively. See animations of the three examples in Movie 1,2 and 3.

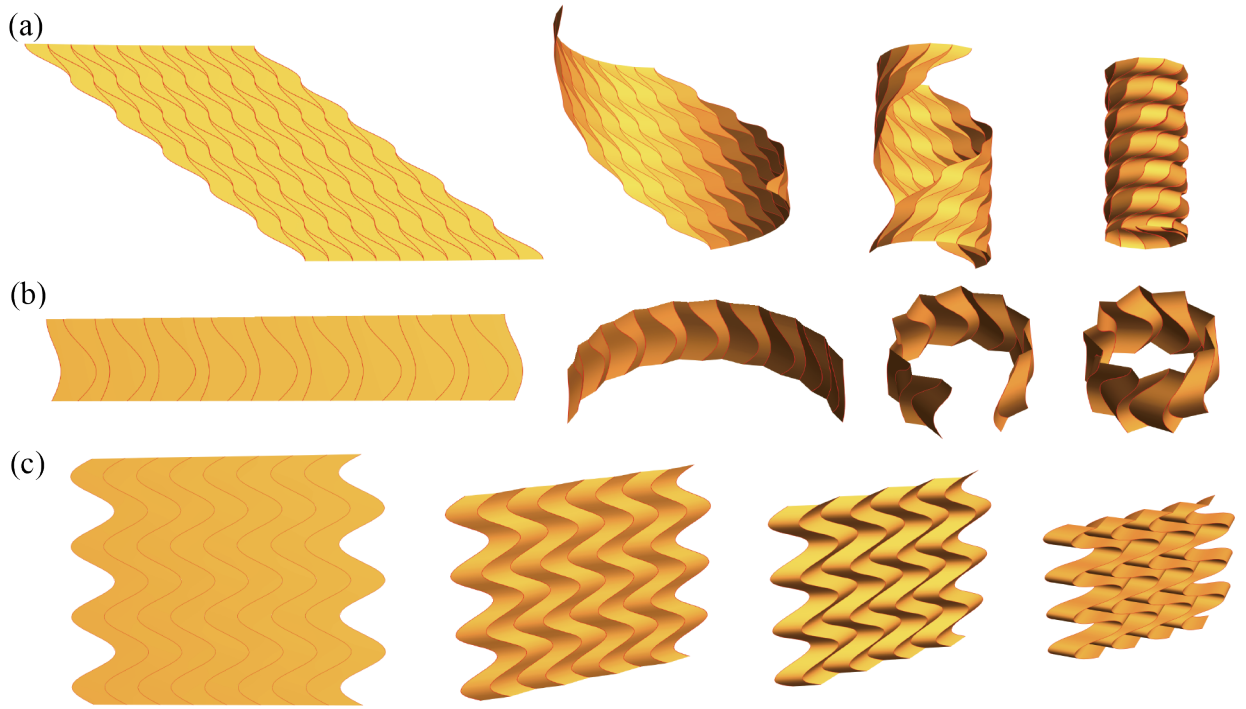


Figure 12: Snapshots of curved origami structures during folding in which (a) helical groups, (b) circle groups, and (c) translation groups are applied at each stage in the folding processes.

In some applications, one would like a flat sheet to fold up spontaneously to one of the deformed structures shown in this paper. This is possible using our results and, for example, a thin sheet of the well-known $\text{Ni}_{50.6}\text{Ti}_{49.4}$ shape memory alloy having martensite as the stable room temperature phase. For this purpose one would begin with a flat stress-free sheet of NiTi at room temperature and deform the sheet isometrically into the desired shape, e.g., one of the deformed shapes shown in this paper. Then, by using a suitable fixture, the sample would be held in that shape. Next, one would apply the standard shape-setting heat treatment for NiTi to this deformed sheet. After cooling to room temperature, removing the fixture and flattening the specimen, heating would cause

the specimen to spontaneously deformed to the folded state, assuming the existence of an energy-decreasing path. A similar but more sophisticated method involving also a preliminary selective etching of creases has been demonstrated in [18]. With suitable measured material properties, the methods of this section are applicable to these cases.

7 Buckling patterns of thin-walled cylindrical and conical shells

In this section we suggest one way to characterize the buckled geometry observed in cylindrical shells and conical shells. In the early work on cylindrical shell buckling [25, 26], workers fitted a thin-walled cylinder onto a mandrel core with a prescribed annular gap, and then compressed the cylinder axially to get a surface texture of diamond-shaped buckles. The Yoshimura origami pattern with straight creases is often used to characterize this buckled geometry [27]. From the experiments shown in [25, 26, 28], we notice that the buckle edges in most patterns are curves rather than straight segments, and the overall layout of buckles is periodic in the axial direction and has rotational symmetry. This structure resembles quite closely our curved origami shown in the bottom left of Figure 5. So, curved origami is potentially useful to describe accurately the buckling patterns. The strategy of constructing such origami structures is given in Algorithm 2. Since the accurate profiles of the buckle edges are not clear, the creases we prescribed to reconstruct buckling patterns are based on our observation. One can choose other curves to better fit the buckle edges according to their experiments.

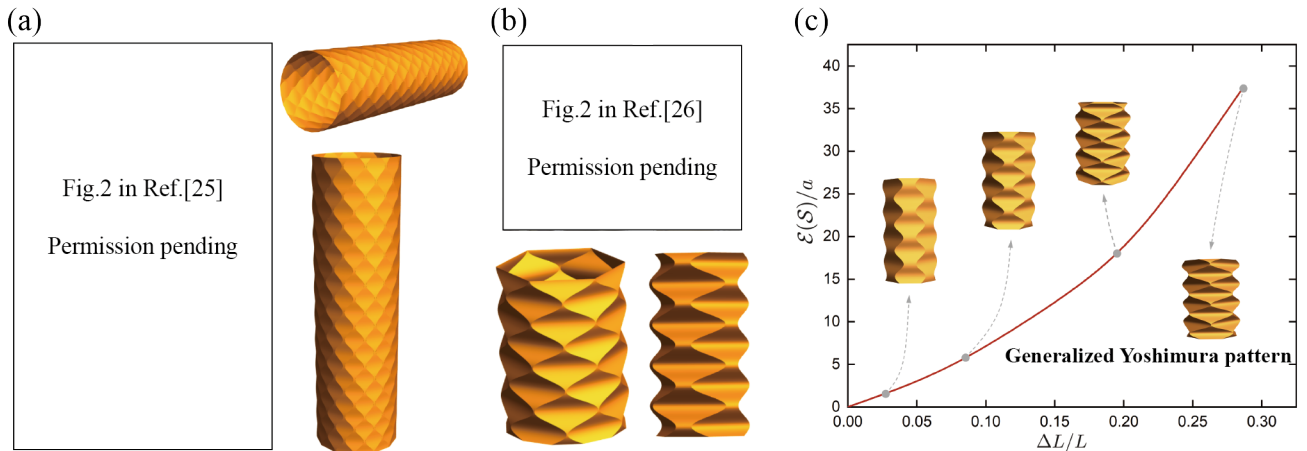


Figure 13: (a) Left: buckling pattern in [25]; Right: curved origami structure resembling the buckling pattern on the left. (b) Top: buckling patterns in [26], where the bumps in the dimples are caused by the mandrel core inside the cylinder; Bottom: curved origami structures resembling the buckling patterns on the top. (c) The stored energy of different buckling patterns of the same thin-walled cylindrical shell, where $a \in \mathbb{R}$ is a constant, L represents the original height of the cylindrical shell and ΔL represents the height of shortening after buckling.

In Figure 13(a) and (b), we rebuild some buckling patterns in [25, 26] with origami structures. Here periodic trigonometric functions are used to characterize the profiles of buckles, which later become the creases of the origami structures. By varying the period and amplitude of the trigonometric function and the number of the creases, one can construct different buckling patterns.

Assuming elasticity theory applies, the energy stored in the buckled surfaces can be found by using Kirchhoff’s plate theory. According to (141), the energy in the buckled cylinder can be found by

$$\mathcal{E}(\mathcal{S}) = \frac{\pi r E h^3}{12} \int_0^H \Lambda(x)^2 dx \quad (156)$$

where r is the radius of the original cylinder, H is the height of the buckled cylinder, and $\Lambda(x)$ is the curvature of the surface curve exactly halfway between two adjacent creases. Figure 13(c) shows the stored energy of different buckling patterns of the same cylindrical shell versus $\Delta L/L$, where L represents original height of the cylindrical shell, $\Delta L = L - H$, and $a = \frac{\pi r E h^3}{12}$. In this plot, each value of $\Delta L/L$ will correspond to a unique buckling pattern since we fix the number of creases and the number of periods of each crease. One can see that the greater the buckling, the more energy is stored. It’s worth mentioning that as the degree of the buckling increases, the two adjacent creases will touch at the peaks, and we will get a generalized Yoshimura pattern (see traditional Yoshimura pattern in [27], where the creases are straight). Note that these curved origami structures are rigid, which is consistent with the observation in experiments. They have different reference crease patterns, not intermediate states of a continuous folding of one crease pattern.

Thin-walled conical shells under uniaxial compression also exhibit diamond-shaped buckles similar to the cylindrical shell case, but the size of the buckles increases gradually from the small radius end to the large radius end [29]. Curved origami also resembles the buckling patterns in this case, and Algorithm 4 is used for the construction since both reference configuration and deformed configuration have rotational symmetry. Figure 14 shows an example to resemble the buckling pattern in [29].

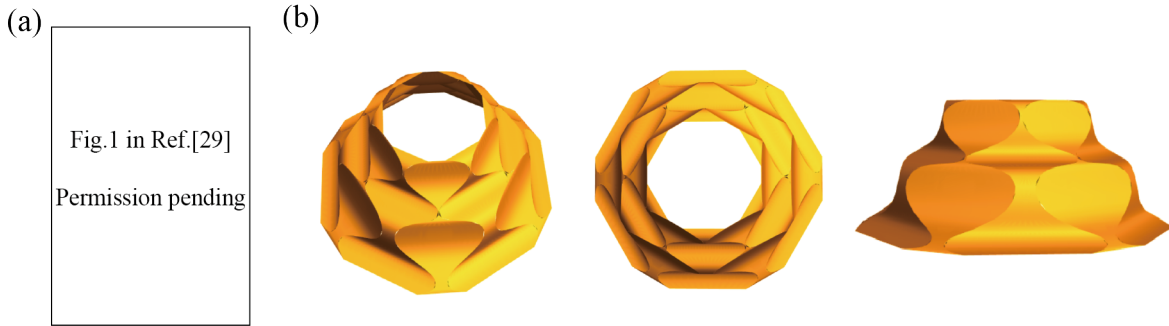


Figure 14: (a) Buckling pattern of the thin-walled conical shell in [29]. (b) Different viewpoints of curved origami structures resembling the buckling pattern of (a).

Acknowledgments The authors acknowledge funding from a Vannevar Bush Faculty Fellowship to RDJ (ONR Grant No. N00014-19-1-2623). The work also benefited from the support of AFOSR (Grant No. FA9550-23-1-0093).

A Appendix

A.1 Proof of Theorem 5.1

Proof. We first prove the necessity. Let the reference creases be $\mathbf{x}_i(s)$, $s_1 < s < s_2$, $1 = 1, 2, \dots, n$, $n > 2$, which are arranged counterclockwise. Let image of $\mathbf{x}_i(s)$ be $\mathbf{y}_i(s)$. Define ruling \mathbf{t}_i , normal \mathbf{n}_i and \mathbf{t}_i^\perp of i^{th} surface bounded by $\mathbf{y}_i(s)$ and $\mathbf{y}_{i+1}(s)$ by

$$\mathbf{t}_i = \frac{\mathbf{y}_{i+1} - \mathbf{y}_i}{|\mathbf{y}_{i+1} - \mathbf{y}_i|}, \quad \mathbf{n}_i = \frac{\mathbf{y}'_i \times \mathbf{t}_i}{|\mathbf{y}'_i \times \mathbf{t}_i|}, \quad \mathbf{t}_i^\perp = \mathbf{n}_i \times \mathbf{t}_i, \quad i = 1, \dots, n, \quad (157)$$

where $\mathbf{y}_{n+1} = \mathbf{y}_1$. \mathbf{t}_i^\perp defined above ensures that

$$\mathbf{t}_{i-1}^\perp \cdot \mathbf{y}'_i < 0 \quad \mathbf{t}_i^\perp \cdot \mathbf{y}'_i < 0. \quad (158)$$

At crease \mathbf{y}_i , we have $\mathbf{n}_{i-1} \cdot \mathbf{y}''_i = -\mathbf{n}_i \cdot \mathbf{y}''_i$, $i = 2, \dots, n$ by (36). Since $(\mathbf{n}_{i-1} \cdot \mathbf{y}'_i)' = (\mathbf{n}_i \cdot \mathbf{y}'_i)' = 0$, we get $\mathbf{n}'_{i-1} \cdot \mathbf{y}'_i = -\mathbf{n}'_i \cdot \mathbf{y}'_i$, that is,

$$(\mathbf{n}'_{i-1} \cdot \mathbf{t}_{i-1}^\perp)(\mathbf{t}_{i-1}^\perp \cdot \mathbf{y}'_i) = -(\mathbf{n}'_i \cdot \mathbf{t}_i^\perp)(\mathbf{t}_i^\perp \cdot \mathbf{y}'_i), \quad i = 2, \dots, n. \quad (159)$$

Thus, if $\mathbf{n}'_i \neq 0$, $\text{sign}(\mathbf{n}'_{i-1} \cdot \mathbf{t}_{i-1}^\perp) = -\text{sign}(\mathbf{n}'_i \cdot \mathbf{t}_i^\perp)$. This means

$$\text{sign}(\mathbf{n}'_1 \cdot \mathbf{t}_1^\perp) = (-1)^{n-1} \text{sign}(\mathbf{n}'_n \cdot \mathbf{t}_n^\perp) = -\text{sign}(\mathbf{n}'_n \cdot \mathbf{t}_n^\perp). \quad (160)$$

Thus, n is even.

Let $\mathbf{F}_i(s)$ be the deformation gradient of the ruling between $\mathbf{y}_i(s)$ and $\mathbf{y}_{i+1}(s)$. According to Corollary 3.4 and Corollary 3.1, the deformation gradients will satisfy

$$\mathbf{F}_1 = \mathbf{P}_1 \mathbf{F}_2, \quad \mathbf{F}_2 = \mathbf{P}_2 \mathbf{F}_3, \quad \dots, \quad \mathbf{F}_{n-1} = \mathbf{P}_{n-1} \mathbf{F}_n, \quad \mathbf{F}_n = \mathbf{P}_n \mathbf{F}_1. \quad (161)$$

where $\mathbf{P}_i = \mathbf{I} - 2\mathbf{b}_i \otimes \mathbf{b}_i$. Thus, we get

$$\mathbf{F}_1 = \mathbf{P}_1 \mathbf{P}_2 \dots \mathbf{P}_n \mathbf{F}_1. \quad (162)$$

Since $\mathbf{P}_1 \mathbf{P}_2 \dots \mathbf{P}_n \in \text{SO}(3)$, we have

$$\mathbf{P}_1 \mathbf{P}_2 \dots \mathbf{P}_n = \mathbf{I}. \quad (163)$$

Therefore, $\mathbf{P}_1 \mathbf{P}_1 \dots \mathbf{P}_n = \mathbf{I}$ and n is even.

Then we show sufficiency. The deformation gradients of the n surfaces are given by

$$\nabla \hat{\mathbf{y}} = \begin{cases} \mathbf{F}_1, & \text{if } \mathbf{x} = (1 - \lambda)\mathbf{x}_1 + \lambda\mathbf{x}_2 \\ \mathbf{P}_2 \mathbf{F}_1, & \text{if } \mathbf{x} = (1 - \lambda)\mathbf{x}_2 + \lambda\mathbf{x}_3 \\ \mathbf{P}_3 \mathbf{P}_2 \mathbf{F}_1, & \text{if } \mathbf{x} = (1 - \lambda)\mathbf{x}_3 + \lambda\mathbf{x}_4 \\ \dots & \dots \\ \mathbf{P}_n \dots \mathbf{P}_3 \mathbf{P}_2 \mathbf{F}_1, & \text{if } \mathbf{x} = (1 - \lambda)\mathbf{x}_n + \lambda\mathbf{x}_1 \end{cases} \quad (164)$$

where $0 < \lambda < 1$. At crease \mathbf{x}_i , $i = 2, \dots, n$, we have

$$\mathbf{y}_i = \mathbf{P}_{i-1} \dots \mathbf{P}_3 \mathbf{P}_2 \mathbf{F}_1 \mathbf{x}'_i = \mathbf{P}_i (\mathbf{P}_{i-1} \dots \mathbf{P}_3 \mathbf{P}_2 \mathbf{F}_1 \mathbf{x}'_i). \quad (165)$$

So the compatibility condition at i^{th} crease is automatically satisfied, $i = 2, \dots, n$. The remaining compatibility condition is at 1st crease. As $\mathbf{P}_n \dots \mathbf{P}_3 \mathbf{P}_2 \mathbf{P}_1 = \mathbf{I}$ and $\mathbf{y}'_1 = \mathbf{F}_1 \mathbf{x}_1 = \mathbf{P}_1 \mathbf{F}_1 \mathbf{x}_1$, we have

$$\mathbf{F}_1 \mathbf{x}'_1 = \mathbf{P}_n \dots \mathbf{P}_3 \mathbf{P}_2 \mathbf{P}_1 \mathbf{F}_1 \mathbf{x}'_1 = \mathbf{P}_n \dots \mathbf{P}_3 \mathbf{P}_2 \mathbf{F}_1 \mathbf{x}'_1, \quad (166)$$

So the n^{th} surface is compatible with the 1st surface at 1st crease. Thus, the curved origami structure is compatible. \square

A.2 Energy stored in a tangent surface

If $\mathbf{x}'_0 \cdot \mathbf{e}^\perp = \mathbf{y}'_0 \cdot \mathbf{t}^\perp = 0$, the developable surface is a tangent surface. Then the rulings and normals are found by

$$\mathbf{e} = \mathbf{x}'_0, \quad \mathbf{t} = \mathbf{y}'_0, \quad (167)$$

$$\mathbf{e}' = \mathbf{x}''_0, \quad \mathbf{e}^\perp = \mathbf{p}_0, \quad (168)$$

$$\mathbf{t}' = \mathbf{y}''_0, \quad \mathbf{t}^\perp = \mathbf{p}, \quad (169)$$

$$\mathbf{n} = \mathbf{t} \times \mathbf{t}^\perp = \mathbf{b}. \quad (170)$$

So $\mathbf{x}''_0 \cdot \mathbf{p}_0 = \mathbf{y}''_0 \cdot \mathbf{p} = \mathbf{e}' \cdot \mathbf{e}^\perp = \mathbf{t}' \cdot \mathbf{t}^\perp$. From (145) we have

$$\begin{aligned} \mathcal{E}_s &= \frac{Eh^3}{24} \int_{s_1}^{s_2} \frac{|\mathbf{n}'|^2}{\mathbf{e}' \cdot \mathbf{e}^\perp} \log\left(\frac{v_2}{v_1}\right) ds, \\ &= \frac{Eh^3}{24} \int_{s_1}^{s_2} \frac{|\mathbf{b}'|^2}{\mathbf{y}''_0 \cdot \mathbf{p}} \log\left(\frac{v_2}{v_1}\right) ds, \\ &= \frac{Eh^3}{24} \int_{s_1}^{s_2} \frac{\tau^2}{\kappa} \log\left(\frac{v_2}{v_1}\right) ds. \end{aligned} \quad (171)$$

References

- [1] Fan Feng, Xiangxin Dang, Richard D James, and Paul Plucinsky. The designs and deformations of rigidly and flat-foldable quadrilateral mesh origami. *Journal of the Mechanics and Physics of Solids*, 142:104018, 2020.
- [2] Huan Liu, Paul Plucinsky, Fan Feng, and Richard D James. Origami and materials science. *Philosophical Transactions of the Royal Society A*, 379(2201):20200113, 2021.
- [3] Fan Feng, Daniel Duffy, Mark Warner, and John S Biggins. Interfacial metric mechanics: stitching patterns of shape change in active sheets. *Proceedings of the Royal Society A*, 478(2262):20220230, 2022.
- [4] Taylor H. Ware, Michael E. McConney, Jeong Jae Wie, Vincent P. Tondiglia, and Timothy J. White. Voxelated liquid crystal elastomers. *Science*, 347(6225):982–984, 2015.
- [5] Robert J Lang. *Origami design secrets: mathematical methods for an ancient art*. CRC Press, 2012.
- [6] Robert J Lang, Erik D Demaine, Klara Mundilova, and Tomohiro Tachi. *Curved folding*. Preprint, 2022.
- [7] Sergio Conti and Francesco Maggi. Confining thin elastic sheets and folding paper. *Archive for Rational Mechanics and Analysis*, 187:1–48, 2008.
- [8] Fan Feng, Paul Plucinsky, and Richard D James. Helical miura origami. *Physical Review E*, 101(3):033002, 2020.

- [9] Lu Lu, Xiangxin Dang, Fan Feng, Pengyu Lv, and Huiling Duan. Conical kresling origami and its applications to curvature and energy programming. *Proceedings of the Royal Society A*, 478(2257):20210712, 2022.
- [10] Stefan Müller and Mohammad Reza Pakzad. Regularity properties of isometric immersions. *Mathematische Zeitschrift*, 251(2):313–331, 2005.
- [11] Sören Bartels and Peter Hornung. Bending paper and the möbius strip. *The Mechanics of Ribbons and Möbius Bands*, pages 113–136, 2016.
- [12] Yaniv Ganor, Traian Dumitrică, Fan Feng, and Richard D James. Zig-zag twins and helical phase transformations. *Philosophical Transactions of the Royal Society A: Mathematical, Physical and Engineering Sciences*, 374(2066):20150208, 2016.
- [13] Huan Liu, Paul Plucinsky, Fan Feng, Arun Soor, and Richard D James. Origami and the structure of materials. *SIAM News*, 55(01), 2022.
- [14] D’Arcy W Thompson. *On growth and form*. Cambridge University Press: Cambridge, 1942.
- [15] Ryan Coulson, Christopher J Stabile, Kevin T Turner, and Carmel Majidi. Versatile soft robot gripper enabled by stiffness and adhesion tuning via thermoplastic composite. *Soft Robotics*, 9(2):189–200, 2022.
- [16] Zirui Zhai, Yong Wang, Ken Lin, Lingling Wu, and Hanqing Jiang. In situ stiffness manipulation using elegant curved origami. *Science Advances*, 6(47):eabe2000, 2020.
- [17] Erik D Demaine, Martin L Demaine, Duks Koschitz, and Tomohiro Tachi. Curved crease folding: a review on art, design and mathematics. In *Proceedings of the IABSE-IASS symposium: taller, longer, lighter*, pages 20–23. Citeseer, 2011.
- [18] Prasanth Velvaluri, Arun Soor, Paul Plucinsky, Rodrigo Lima de Miranda, Richard D James, and Eckhard Quandt. Origami-inspired thin-film shape memory alloy devices. *Scientific reports*, 11(1):1–10, 2021.
- [19] Joseph Choma. *Morphing: A Guide to Mathematical Transformations for Architects, Designers*. Hachette UK, 2015.
- [20] Huan Liu, Kalpesh Jaykar, Vinitendra Singh, Ankit Kumar, Kevin Sheehan, Peter Yip, Philip Buskohl, and Richard D James. Options for dynamic similarity of interacting fluids, elastic solids and rigid bodies undergoing large motions. *Journal of Elasticity*, pages 1–19, 2023.
- [21] Fan Feng, Paul Plucinsky, and Richard D James. Phase transformations and compatibility in helical structures. *Journal of the Mechanics and Physics of Solids*, 131:74–95, 2019.
- [22] T Hahn. *International tables for crystallography: volumes A,E*. Kluwer Academic Publishers, 2003.
- [23] Gero Friesecke, Richard D James, and Stefan Müller. A theorem on geometric rigidity and the derivation of nonlinear plate theory from three-dimensional elasticity. *Communications on Pure and Applied Mathematics*, 55(11):1461–1506, 2002.

- [24] Erwin Kreyszig. *Introduction to differential geometry and Riemannian geometry*. University of Toronto Press, 2019.
- [25] WH Horton and SC Durham. Imperfections, a main contributor to scatter in experimental values of buckling load. *International Journal of Solids and Structures*, 1(1):59–72, 1965.
- [26] KA Seffen and SV Stott. Surface texturing through cylinder buckling. *Journal of Applied Mechanics*, 81(6), 2014.
- [27] Giles W Hunt and Ichiro Ario. Twist buckling and the foldable cylinder: an exercise in origami. *International Journal of Non-Linear Mechanics*, 40(6):833–843, 2005.
- [28] Eugene E Lundquist. Strength tests of thin-walled duralumin cylinders in compression. Technical report, 1934.
- [29] VI Weingarten, EJ Morgan, and Paul Seide. Elastic stability of thin-walled cylindrical and conical shells under axial compression. *AIAA Journal*, 3(3):500–505, 1965.